# MR Thermometry

Le Zhang

LeZh@mednet.ucla.edu

M229

May 9, 2019


David Geffen
School of Medicine

UCLA
Magnetic Resonance Research Labs

UCLA Radiology

# Why Thermometry with MR?

- Accurate temperature measurement is critical for successful implementation of thermal therapies

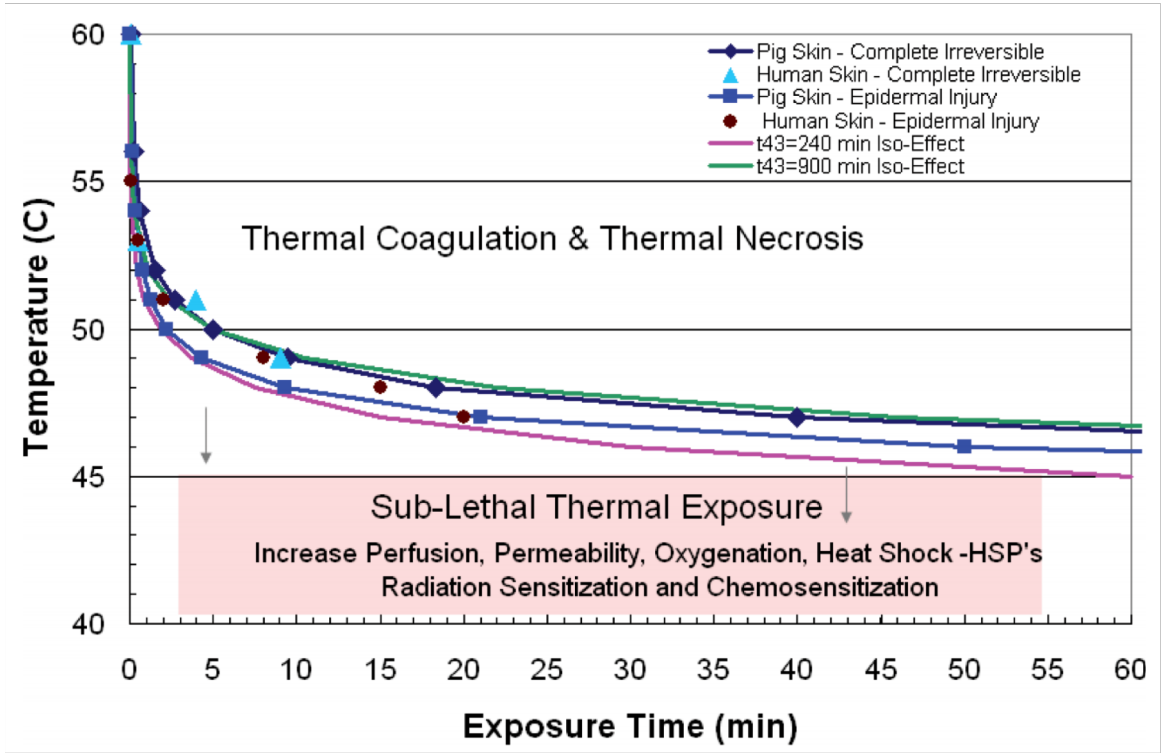




Diederich, CJ, *Int. J. Hyperthermia*, 2015

# Why Thermometry with MR?

- During High-Intensity Focused Ultrasound (HIFU) treatment sessions, it is even more important to be able to relate treatment temperature to actual thermal tissue damage

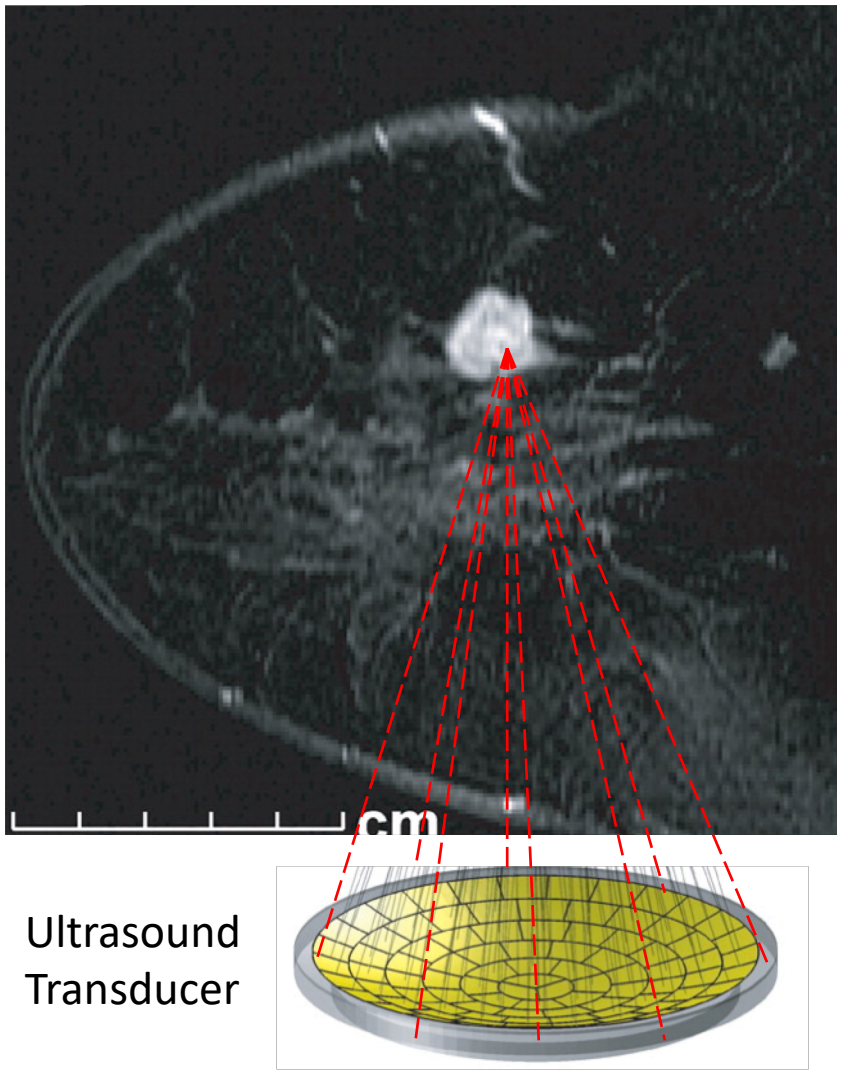


Tempeny, CMC, *Radiology*, 2011

# Why Thermometry with MR?

- Invasive thermometry methods can have severe complications such as hemorrhage, infections and/or pain

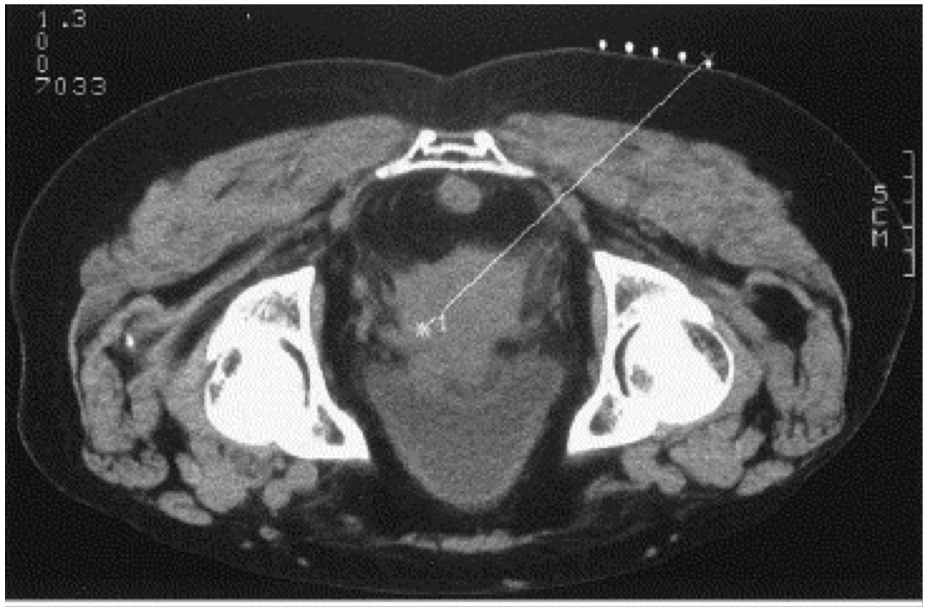

CT-guided Insertion of Thermal Probe

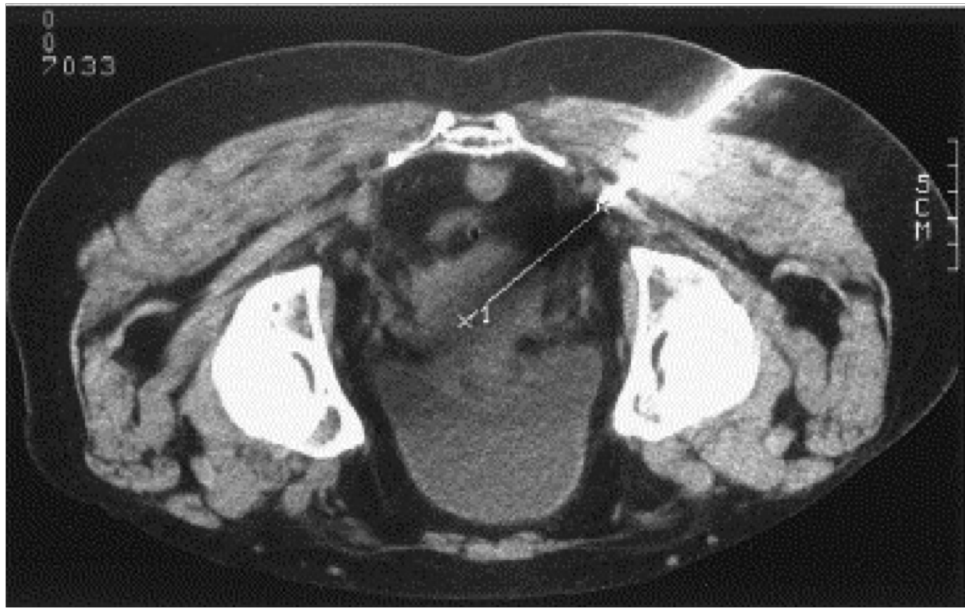

David Geffen School of Medicine

van der Zee, J, *Int J Radiat Oncol Biol Phys*, 1998

# Why Thermometry with MR?

- MRI has a wider coverage, and it can also provide anatomical references to guide treatment

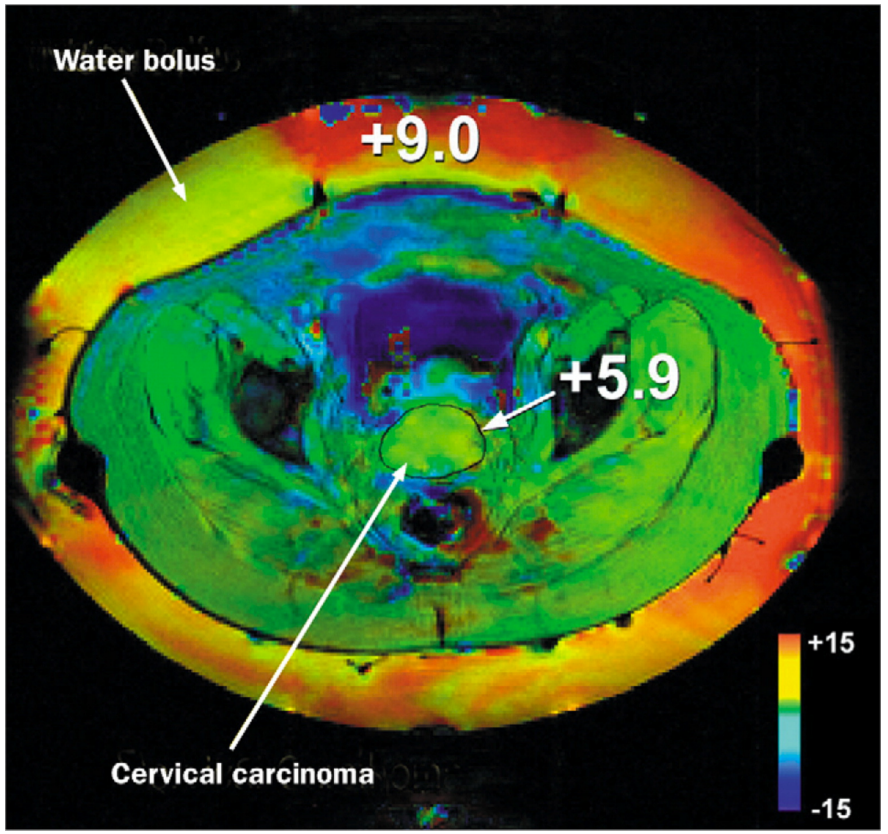




Wust, P, *Lancet Oncol*, 2002

# MRI: What to Measure Temperature With?

*What contrast does MRI provide?*

- Proton density
- $T_1$
- $T_2$
- $T_2^*$
- Apparent diffusion coefficient
- Chemical shift
- Magnetization transfer

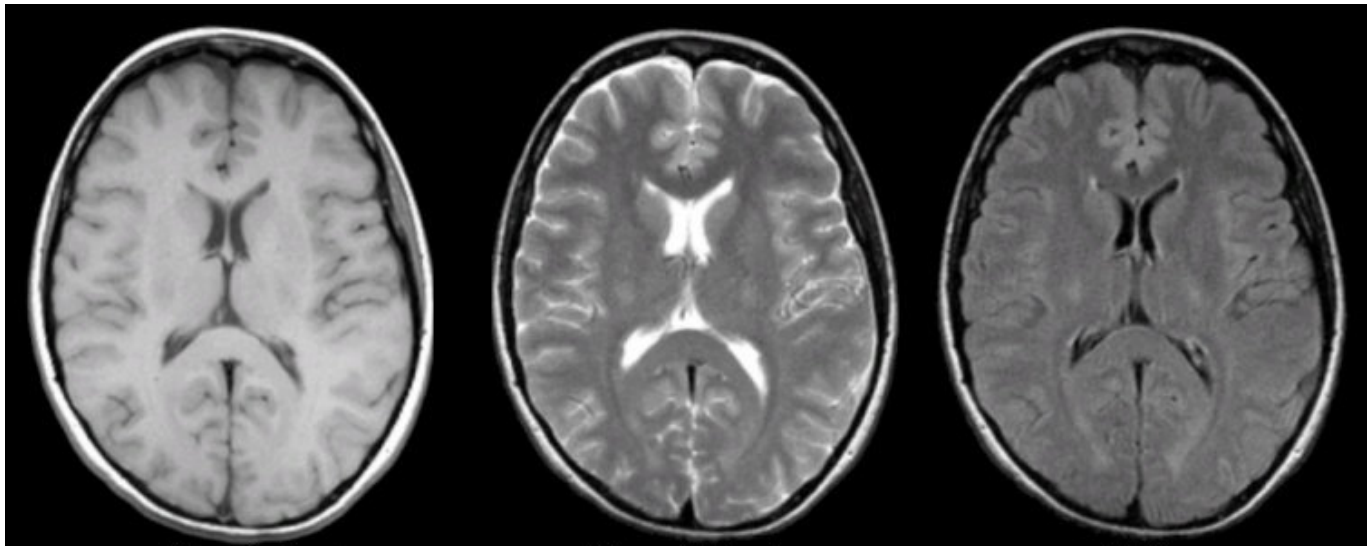

*Turns out, they are all temperature dependent!*

# MR Thermometry with Proton Density

- Proton density ($M_0$) obeys Boltzmann Distribution

$$M_0 = N\frac{\gamma^2 h^2 B_0}{4\mu_0 kT} \propto \frac{1}{T}$$

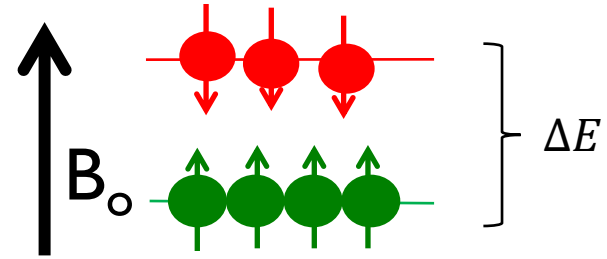


- Between 37 and 80°C, PD decreases linearly with temperature at a rate of (-0.30±0.01)%/°C

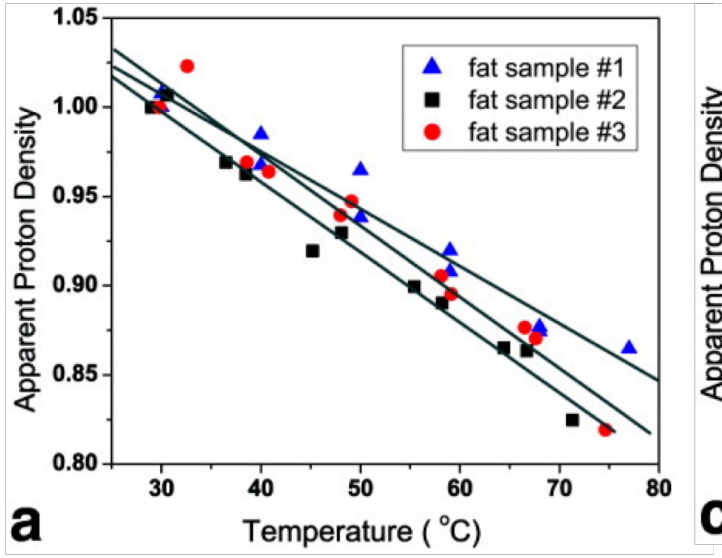


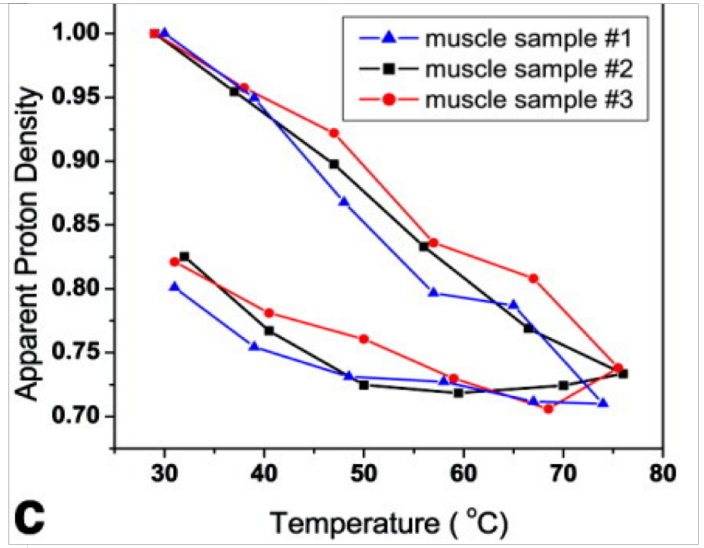




Chen J. *J Magn Reson Imaging,* 2006

# MR Thermometry with $T_1$

- The spin-lattice relaxation stems from the dipolar interaction between molecules, a process that requires overcoming an activation energy $E_a$

$$T_1(T) \propto e^{-E_a(T_1)/kT} \approx T_1(T_{ref}) + m \cdot (T - T_{ref})$$

- The temperature coefficient is determined empirically for different tissue types. $T_1$ generally increases by 1%/°C, with some tissue variation

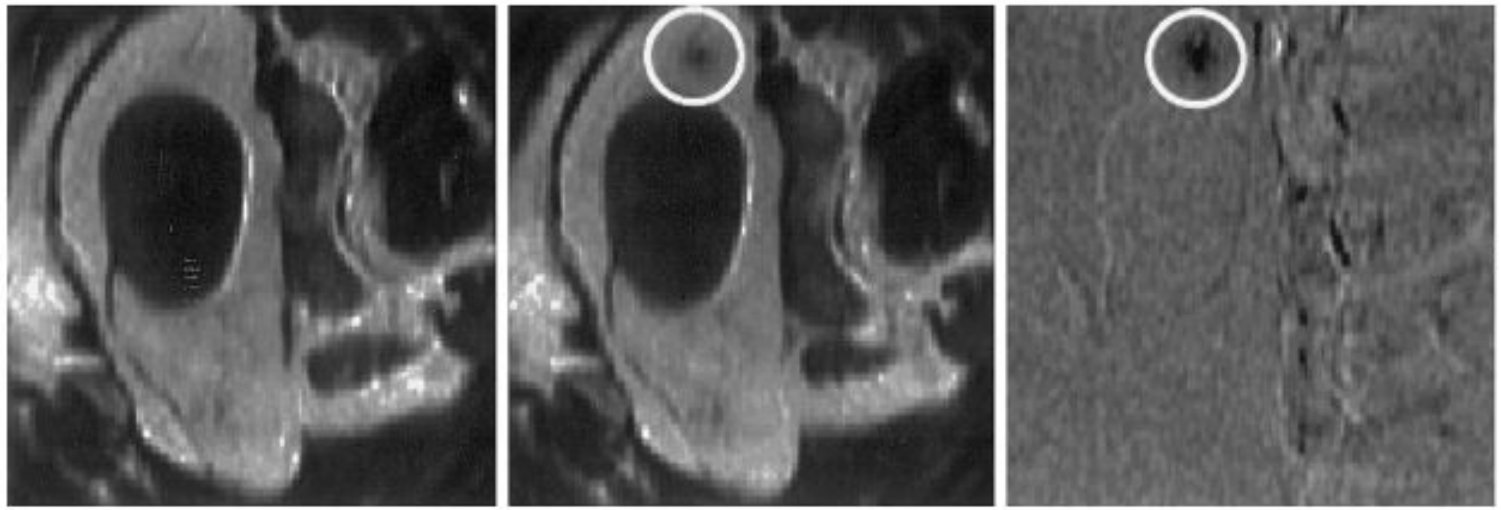



Hynynen K, *Magn Reson Med* 2000

# MR Thermometry with $T_1$: Weighted Imaging

- For both spin echo and gradient echo sequences, the change in $T_1$ signal intensity at an unknown temperature T with respect to a reference temperature $T_{ref}$ due to temperature can be modeled as

$$\frac{\mathrm{d}S}{S\mathrm{d}T} = -\frac{m\mathrm{TR}(1-cos\alpha)E_1}{T_1T_{ref}^2(1-E_1)(1-E_1cos\alpha)} - \frac{1}{T_{ref}}$$

where

$$E_1 = \exp[-\frac{TR}{T_1T_{ref} + m(T-T_{ref})}]$$

# MR Thermometry with $T_1$: Mapping Method

- $T_1$ can be determined by using inversion-recovery method, but it can be very time-consuming.
- The temperature dependence of $T_1$ is also varies with tissue type.

**Table 2.** $T_1$ temperature dependence (in ms/°C) at a given initial temperature $T_0$. For the individual samples, '±' denotes the standard deviation ($n$ = 30) over the voxels of the region of interest (ROI). For the average value, '±' denotes the standard deviation over the mean of the seven samples

| Sample | $T_0$ = 25 °C | $T_0$ = 35 °C | $T_0$ = 45 °C | $T_0$ = 55 °C | $T_0$ = 65 °C |
|---|---|---|---|---|---|
| 1, heating | 5.39 ± 0.09 | 6.28 ± 0.14 | 7.23 ± 0.20 | 8.24 ± 0.27 | 9.30 ± 0.36 |
| 1, cooling | 5.38 ±0.10 | 6.26 ±.0.13 | 7.20 ±0.16 | 8.20 ± 0.21 | 9.25 ± 0.27 |
| 1, extracted fat | 5.48 ±0.12 | 6.41 ± 0.18 | 7.41 ±0.25 | 8.47 ± 0.33 | 9.60 ± 0.43 |
| 2, heating | 5.45 ± 0.07 | 6.39 ± 0.14 | 7.41 ± 0.24 | 8.49 ± 0.36 | 9.64 ± 0.50 |
| 3, heating | 5.25 ± 0.14 | 6.23 ± 0.22 | 7.29 ± 0.31 | 8.44 ± 0.43 | 9.67 ± 0.58 |
| 4, heating | 5.40 ± 0.05 | 6.35 ± 0.12 | 7.38 ± 0.10 | 8.47 ± 0.15 | 9.63 ± 0.21 |
| 4, cooling | 5.40 ± 0.09 | 6.27 ± 0.12 | 7.20 ± 0.17 | 8.18 ± 0.23 | 9.21 ± 0.31 |
| 5, heating | 5.24 ± 0.15 | 6.14 ± 0.20 | 7.10 ± 0.27 | 8.13 ± 0.35 | 9.22 ± 0.45 |
| 6, heating | 5.34 ± 0.06 | 6.28 ± 0.09 | 7.31 ± 0.13 | 8.40 ± 0.19 | 9.57 ± 0.27 |
| 7, heating | 5.36 ± 0.09 | 6.30 ± 0.14 | 7.32 ± 0.21 | 8.41 ± 0.28 | 9.57 ± 0.37 |
| Average ($n$ = 7) (of heating) | 5.35 ± 0.08 | 6.28 ± 0.08 | 7.29 ± 0.09 | 8.36 ± 0.12 | 9.50 ± 0.16 |



Baron P, *NMR Biomed* 2015

# MR Thermometry with $T_1$: Mapping Method

- Variable flip angle (VFA) method can serve as a faster alternative for $T_1$ mapping
  - Flip angles are chosen such that they generate 70% of the Ernst angle signal magnitude, enabling faster mapping
  - $B_1$ map is required to correct for flip angle errors
  - $T_1$ can be calculated by fitting the MR signal intensity and flip angle $\vartheta$ with

$$S = M_0 \frac{\left(1 - e^{-TR/T_1}\right) sin\theta}{1 - e^{-TR/T_1}\, e^{-TR/T_2^*} - \left(e^{-TR/T_1} - e^{-TR/T_2^*}\right) cos\theta}$$

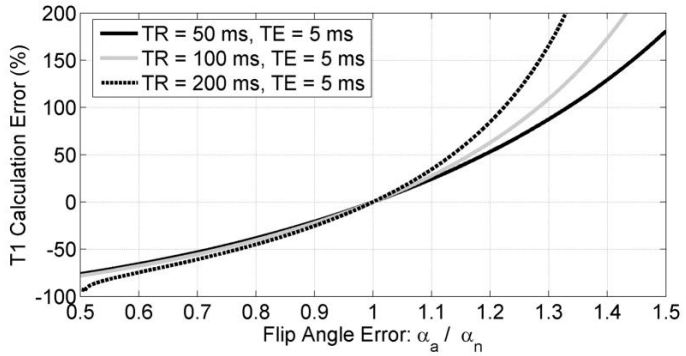


$T_1$ Error Caused by Imperfect Flip Angle

Todd N, *Magn Reson Med,* 2013

# MR Thermometry with $T_1$: Steady State

We record $M_x$, $M_y$ and Mz as a ratio against the initial magnetization $M_0$

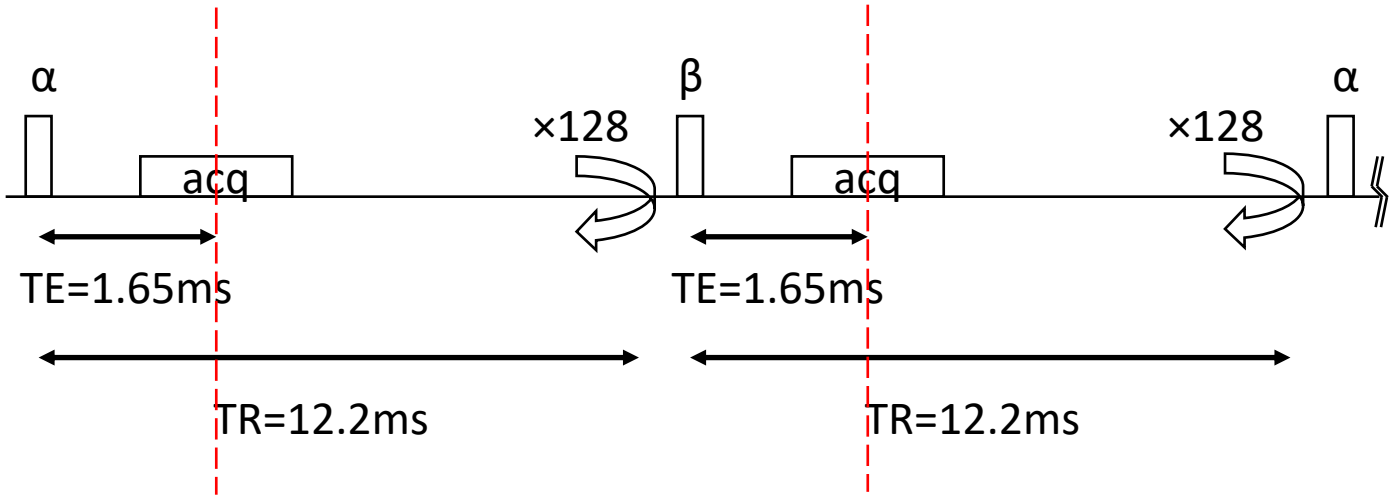


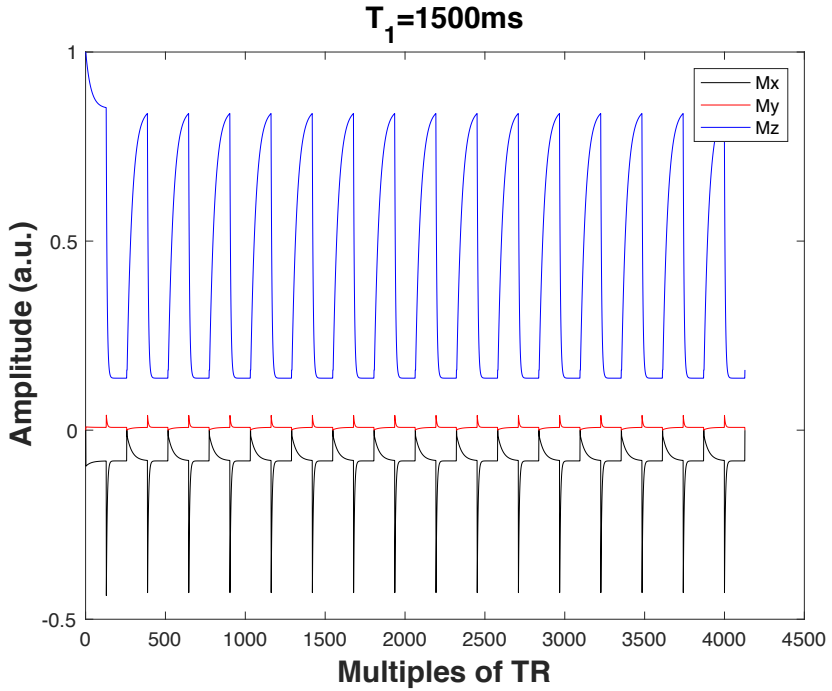


- Spoiled GRE Acquisition, TR=12.2ms, TE=1.65ms, $T_2$=100ms
- For spins with short $T_1$ (i.e. fat), SS is established much faster for both flip angles.

# MR Thermometry with $T_2$

- Temperature dependence of $T_2$ has a similar origin as $T_1$.
- However, $T_2$ of water in tissue can be easily masked by other factors
- An “apparent” $T_2$ can be used instead to measure temperature change

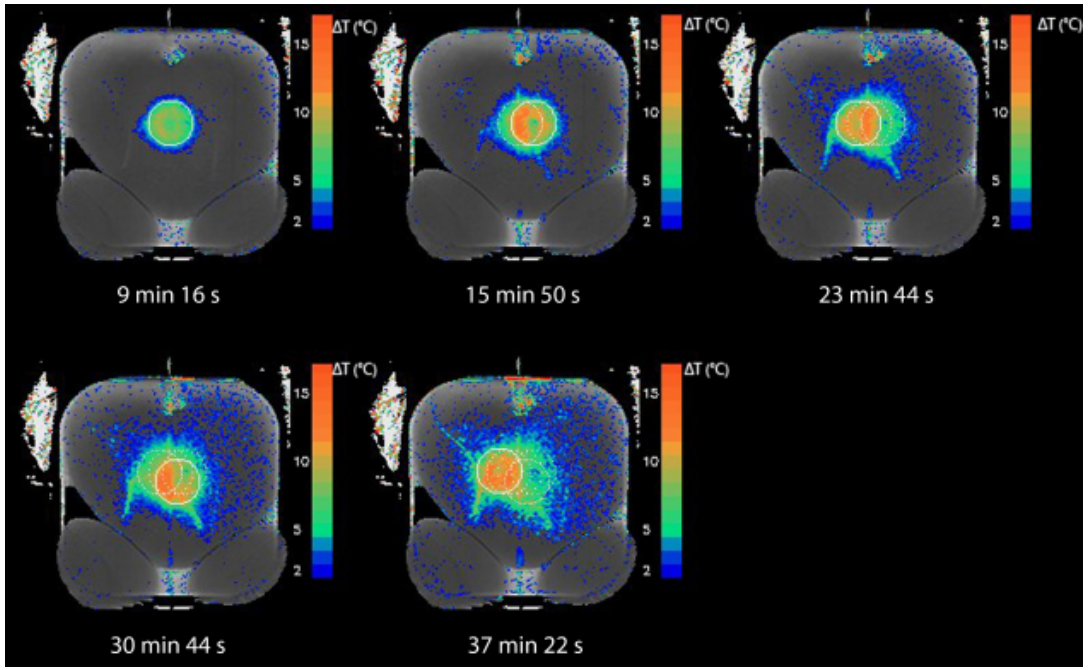




Baron P, *Magn Reson Med*. 2014

# MR Thermometry with Diffusion

- Using the same approach, assuming the activation energy of free diffusion is $E_a(D)$

$$T = T_0 + \frac{kT_0^2}{E_a(D)} \frac{D - D_0}{D_0}$$

- The temperature sensitivity of ADC is high at 2%, but it can become non-linear when tissue condition changes induce barriers
- Full diffusion tensor imaging can be necessary due to diffusion anisotropy



Rieke V, Pauly KB. J Magn Reson Imaging 2008; 27: 376-390

# MR Thermometry with PRF

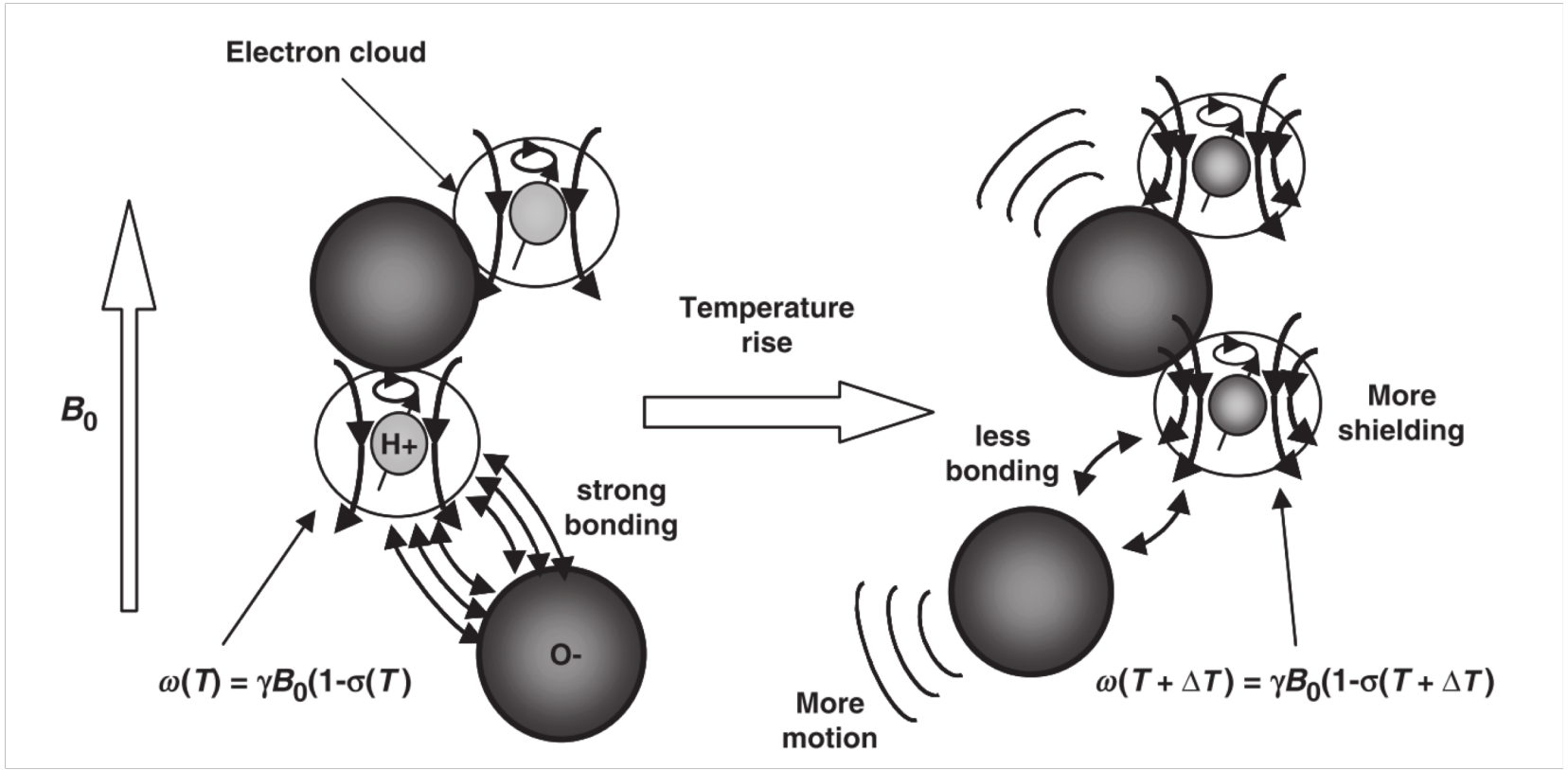


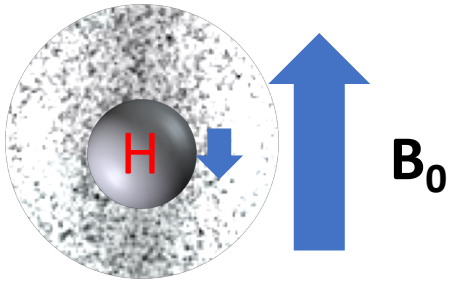


$$\omega = \gamma B_0(1-s)$$

*s* is called the shielding constant, and it increases linearly with temperature between -15 and 100°C at a rate of $0.01\times10^{-6}$/°C as hydrogen bonds bend, twist, or break.



Kuroda K. *Int J Hyperthermia*, 2005

# MR Thermometry with PRF

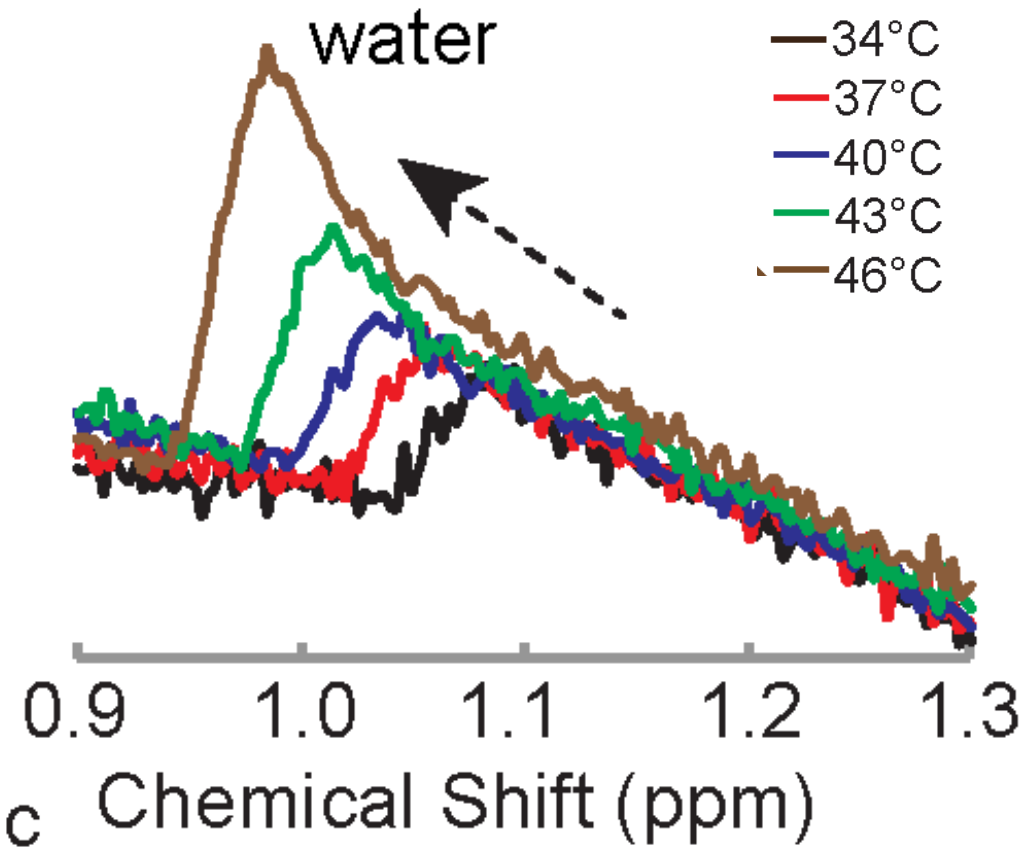


$$\Delta\phi = TE \cdot \Delta f$$

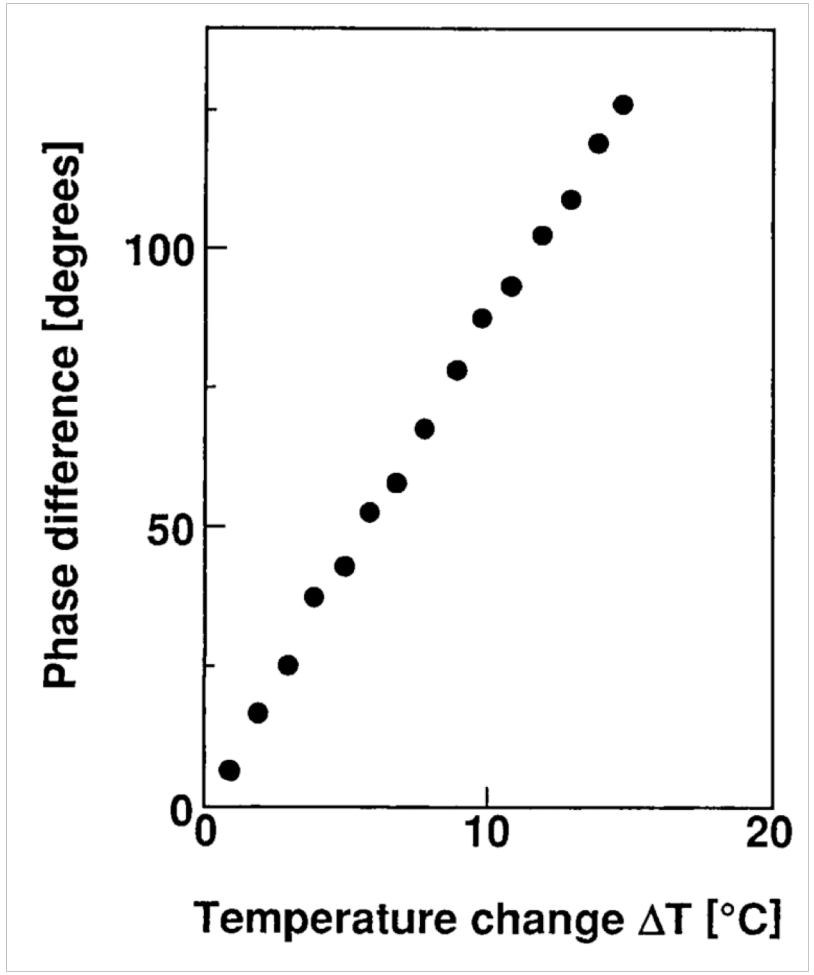

# PRF Thermometry: Pitfalls

| Parameter | | Value | |
|---|---|---|---|
| **Static magnetic field** | $dB_0/dt$ | **Field drift** | 0.02 ppm/h |
| **Chemical shift** | $d\delta/dT$ | **Pure water** | −0.01 ppm/°C |
| | | **Tissue (except fat)** | −(0.009–0.01) ppm/°C |
| | | **Fat** | −0.00018 ppm/°C |
| **Permittivity** | $d\varepsilon/dT$ | **Water** | −0.5%/°C |
| **Electrical conductivity** | $d\sigma_{el}/dT$ | **Dog muscle** | 1.7%/°C |
| **Permeability** | $d\mu/dT$ | **Water** | 3.10−7%/°C |
| **Magnetic susceptibility** | $d\chi/dT$ | **Pure water** | 0.0026 ppm/°C (30–45 °C) |
| | | **Muscle** | 0.0016 ppm/°C (30–45 °C) |
| | | **Breast fat** | 0.0039–0.0076 ppm/°C |
| | | **Air** | −0.002 ppm/°C |



Winter L. *Int J Hyperthermia*, 2016

# MR Thermometry with PRF: Spectroscopic Approach

- A temperature independent peak is commonly used as a reference to correct for the effect of motion, field drift and/or field inhomogeneities on PRF
- This peak can be the fat (methylene) proton peak in the body, or the NAA proton peak in the brain
- Chemical shift image (CSI), echo planar spectroscopic imaging (EPSI), line scan echo planar spectroscopic imaging (LSEPI) or water saturation shift referencing methods can be used
- But this approach tends to be very slow, with poor resolution



Rieke V, *J Magn Reson Imaging*, 2008

# Spectroscopic MR Thermometry with PRF

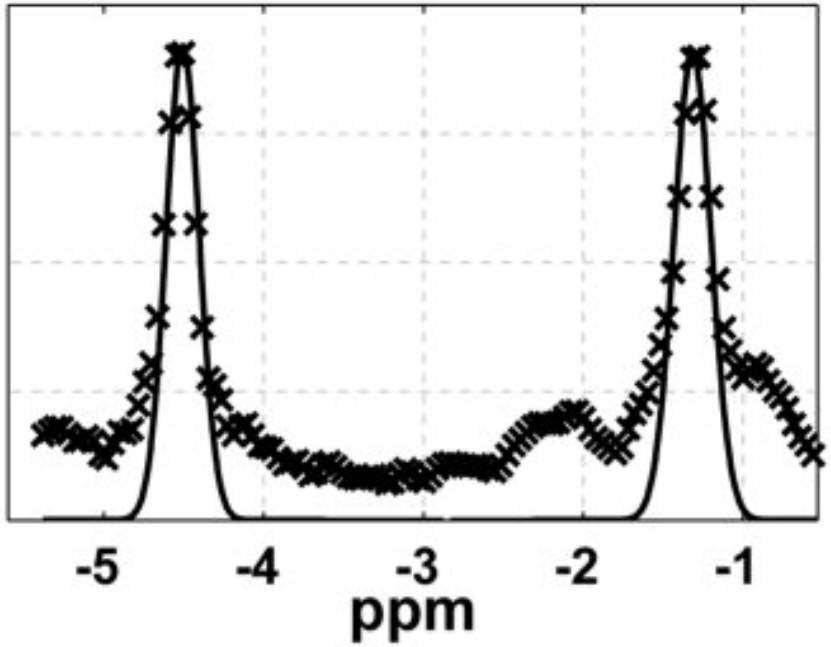


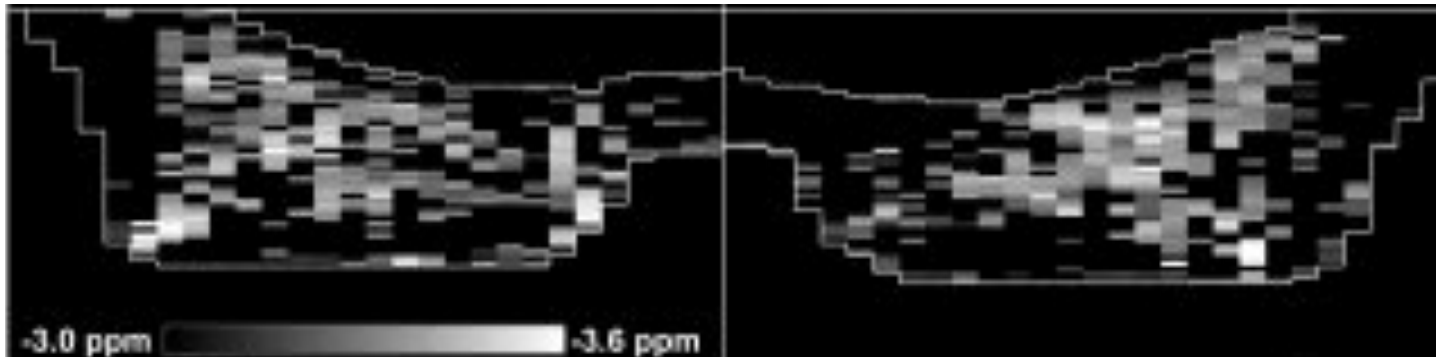


- LSEPSI method
- Human subject imaging
- 2.5*mm* in-plane resolution
- 6.5*s* scanning time per slice



MacDonnald N,. *Magn Reson Med* 2007

# Spectroscopic MR Thermometry with Other Nuclei

TmDOTP5$^{-}$

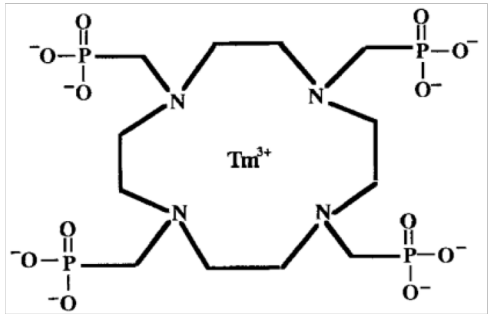


Temperature Dependence of $^{31}$P Peak

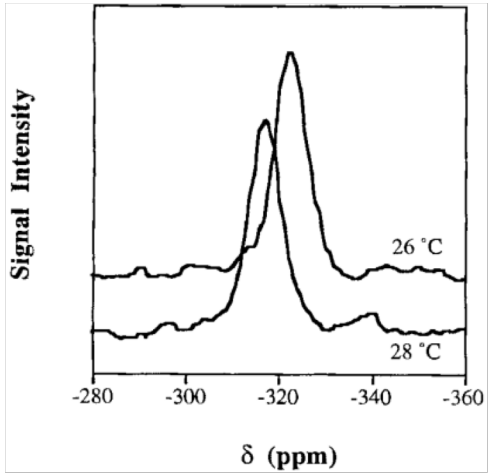


- Both $^{31}$P and $^{129}$Xe have higher temperature sensitivities than PRF
- Due to low natural abundance, these methods yield low SNR, long scanning time and generally are confined to spectroscopic imaging

Encapsulated $^{129}$Xe

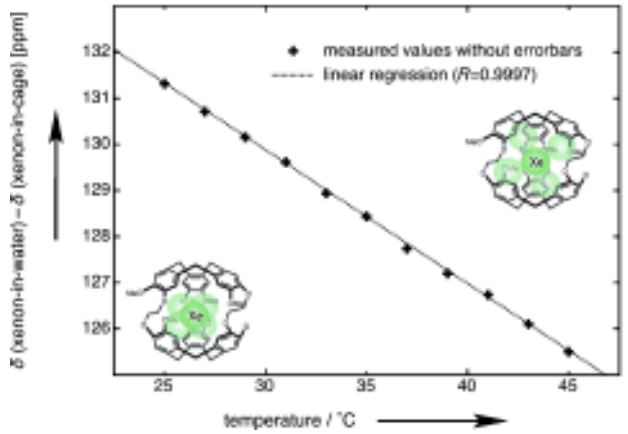


$$\delta_2[ppm] - \delta_1[ppm] = -0.29ppm/°C \times T[°C] + 138.57[ppm]$$

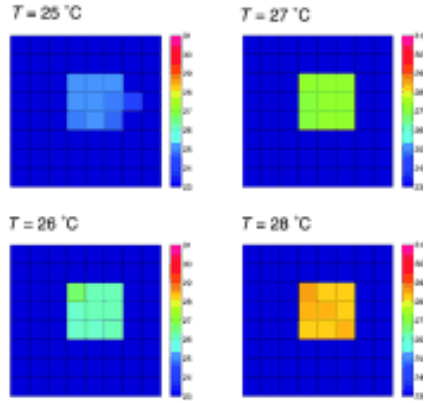


Zuo CS, *Magn Reson Med*, 1996
Schilling F, *Magn Reson Med*, 2010

# MR Thermometry with PRF: Phase Mapping Approach

Wrapped Phase Map

Unwrapped Phase Map

Phase Difference Map

Pre-treatment temperature (or reference temperature $T_0$)

Unknown, elevated temperature ($T$)

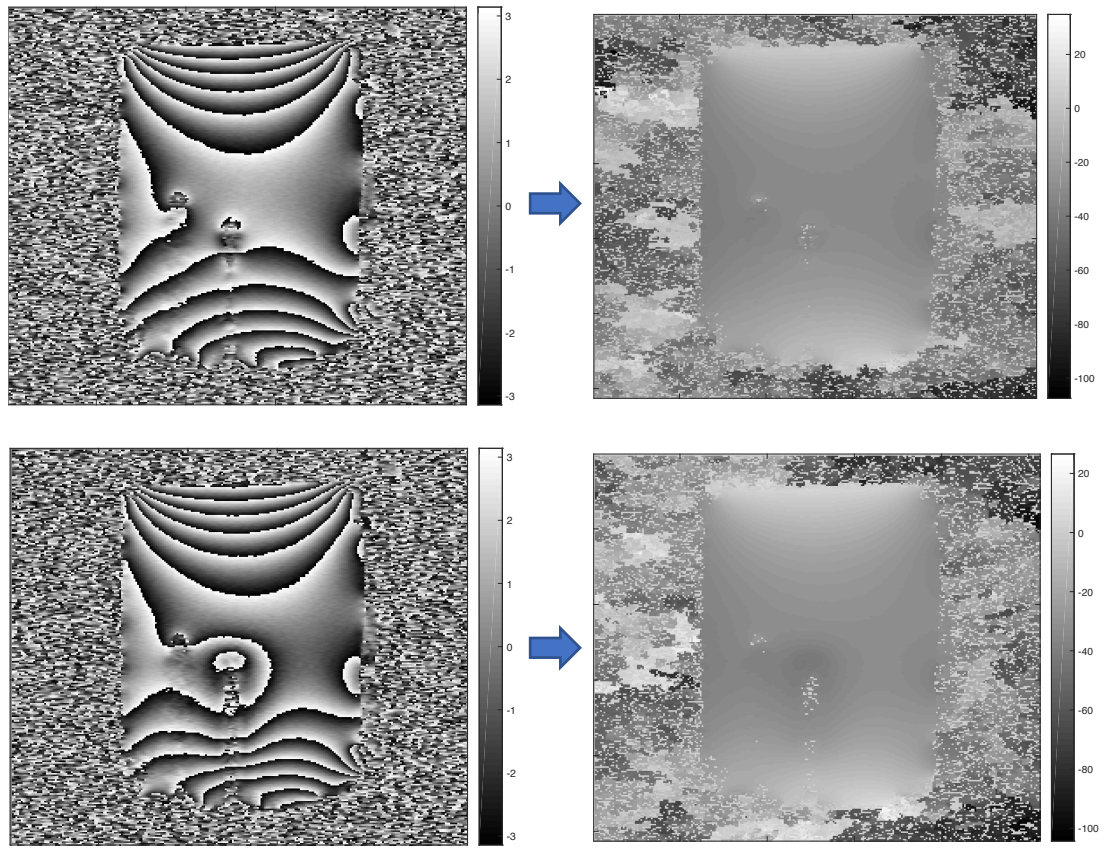

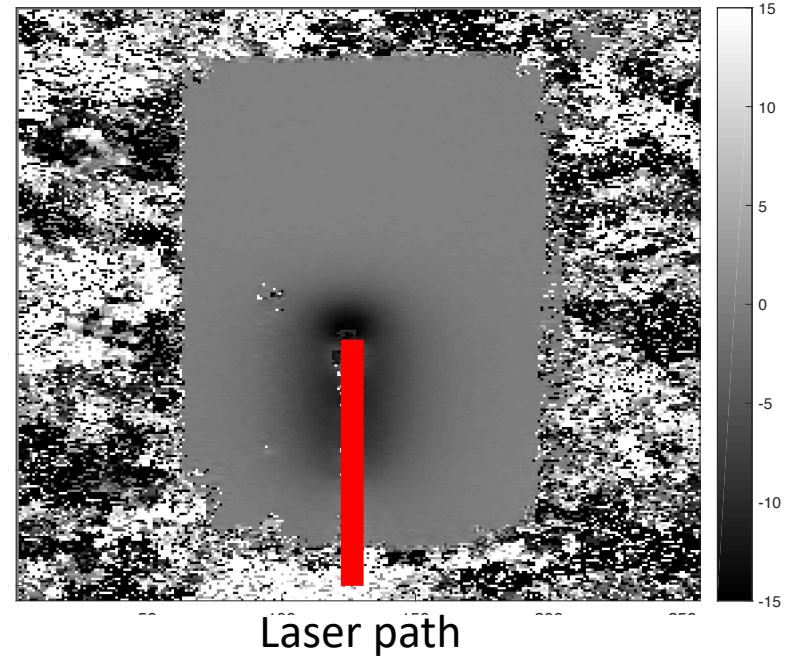

Laser path

# MR Thermometry with PRF: Phase Mapping Approach

- The estimate of *T* can thus be calculated as, with $\alpha$=-0.01ppm/°C

Phase Difference Map

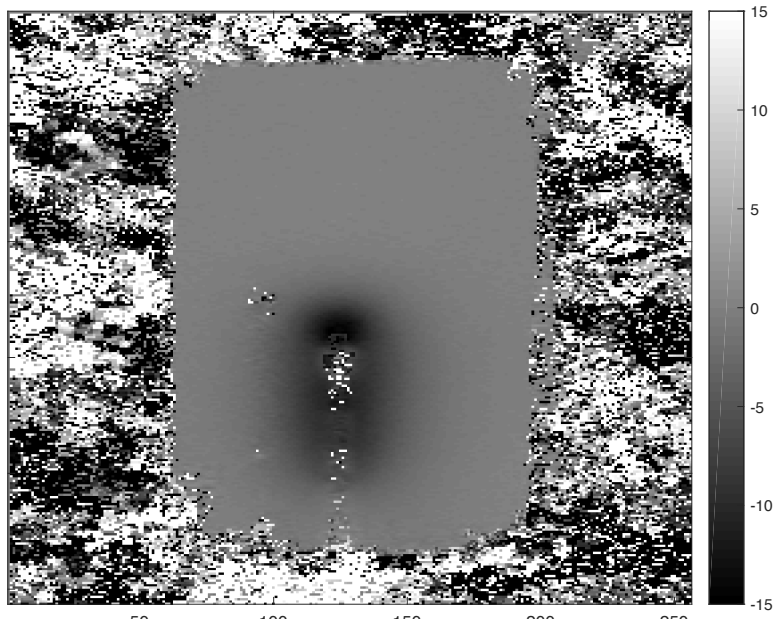


$$\Delta T = \frac{\phi(T) - \phi(T_0)}{\gamma \alpha B_0 TE}$$

Relative Temperature Change Map

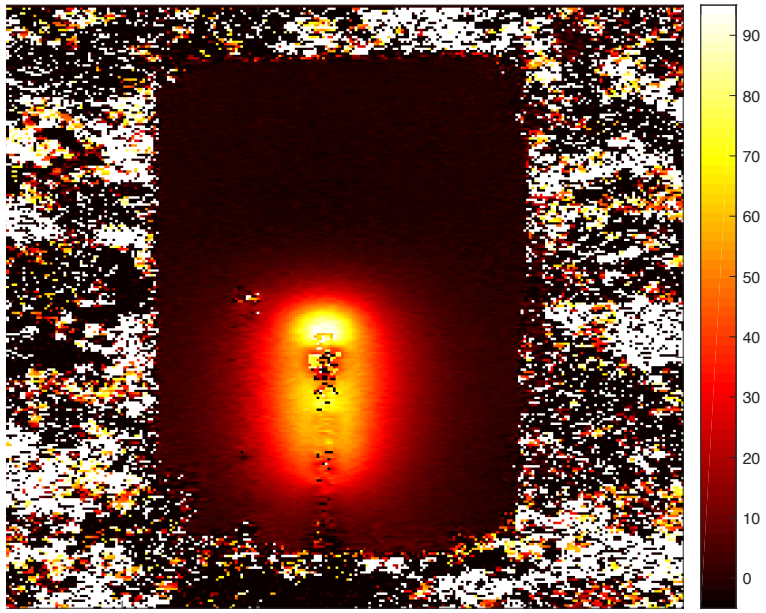




Ishihara Y, Calderon A, Watanabe H, et al. Magn Reson Med 1995; 34: 814-823

# MR Thermometry with PRF: Choice of TE

Echo Time

Less relaxation; higher SNR
Lower TR; faster acquisition

More “fanning out” of the spin;
better temperature accuracy

- In a gradient echo sequence, the SNR of the phase difference between two images acquired at different temperature $\Delta\phi(\Delta T)$ is directly proportional to the signal intensity *A*: $SNR_{\Delta\phi} = |\Delta\phi(\Delta T)| \cdot A$
- Which is in turn: $SNR_{\Delta\phi} \propto TE \cdot e^{-TE/T_2^*}$
- Differentiating the above expression gives the optimal TE as $TE = T_2^*$

# PRF Thermometry Pitfalls: Motion & Multibaseline Correction

Temperature Error due to Motion

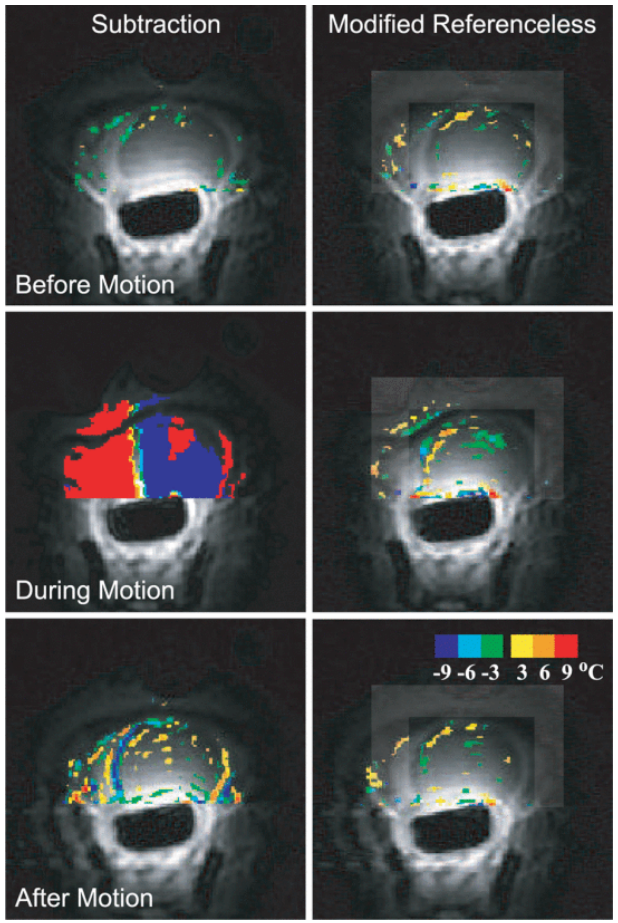


Multiple baseline images are acquired during one motion cycle

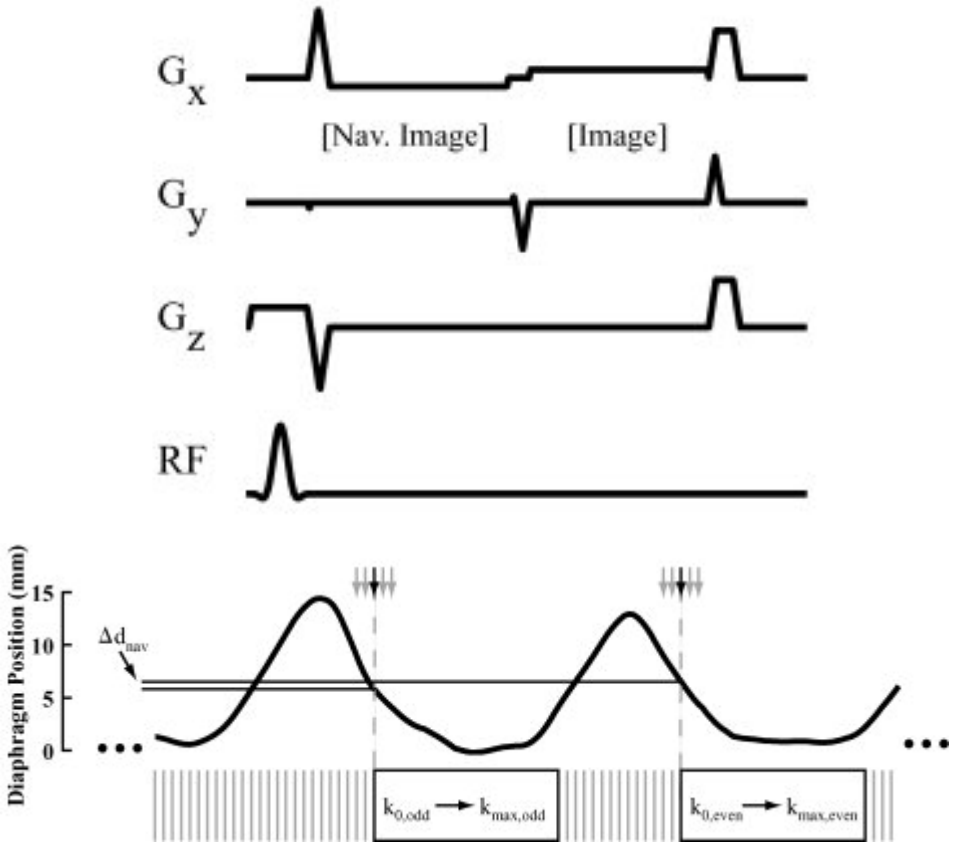


Each line in *k*-space is matched with a baseline from the library

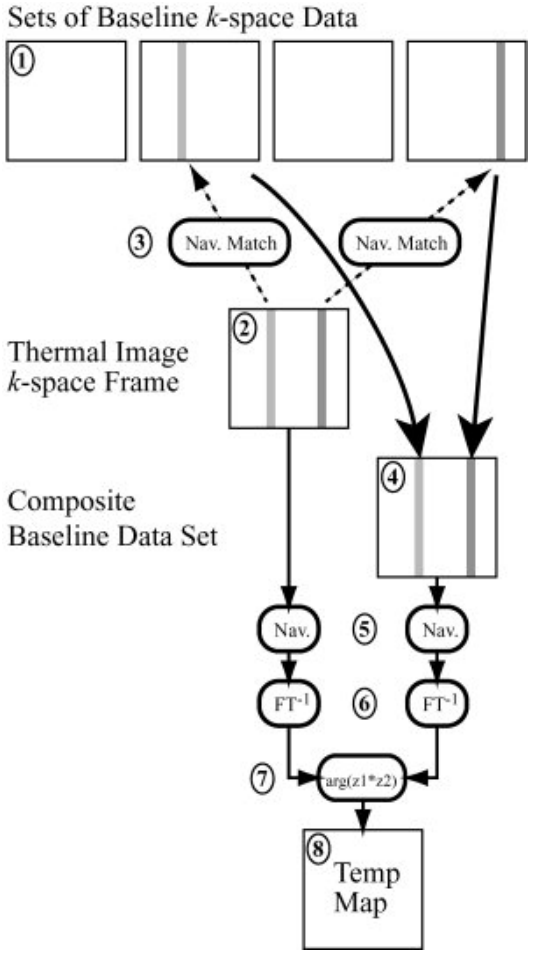




Rieke V, *IEEE Trans Med Imaging*, 2007
Vigen KK, *Magn Reson Med*, 2003

# PRF Thermometry Pitfalls: Phase of Fat

- The temperature independence of fat peak complicates phase mapping

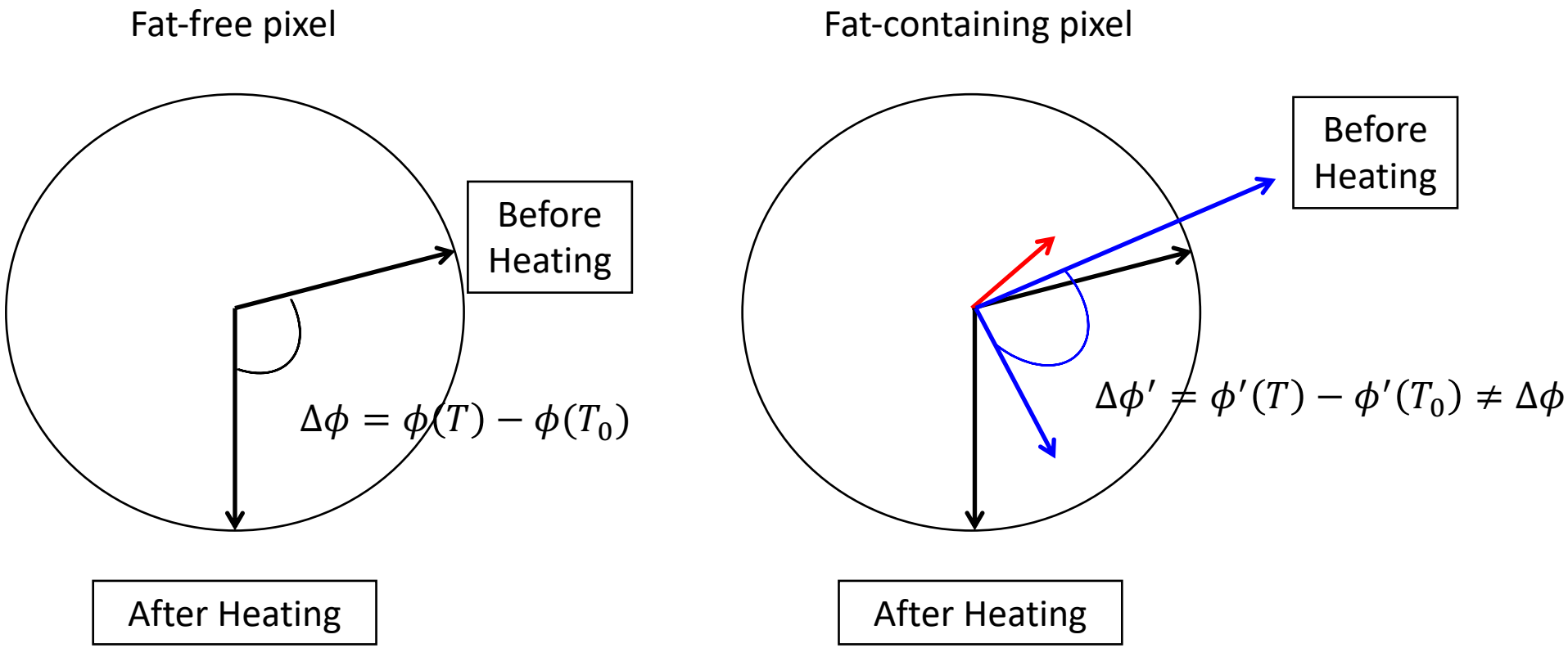

# PRF Thermometry Pitfalls: Magnetic Susceptibility

- The localized magnetic field a nucleus feels deviates from the macroscopic $B_0$ field depending on its magnetic susceptibility

$$B_{nuc} \cong \mathrm{B}_{mac} - \left(\frac{2}{3}\chi + \sigma\right) B_0$$

- The error in temperature measurement can be

$$\epsilon_T = -\frac{1}{\alpha}\left(\frac{\Delta B_{mac}}{B_0 \Delta T} - \frac{2}{3}\frac{\Delta \chi}{\Delta T}\right)$$

- Susceptibility of fat also changes with temperature with a rate similar to PRF, further compounding the problem

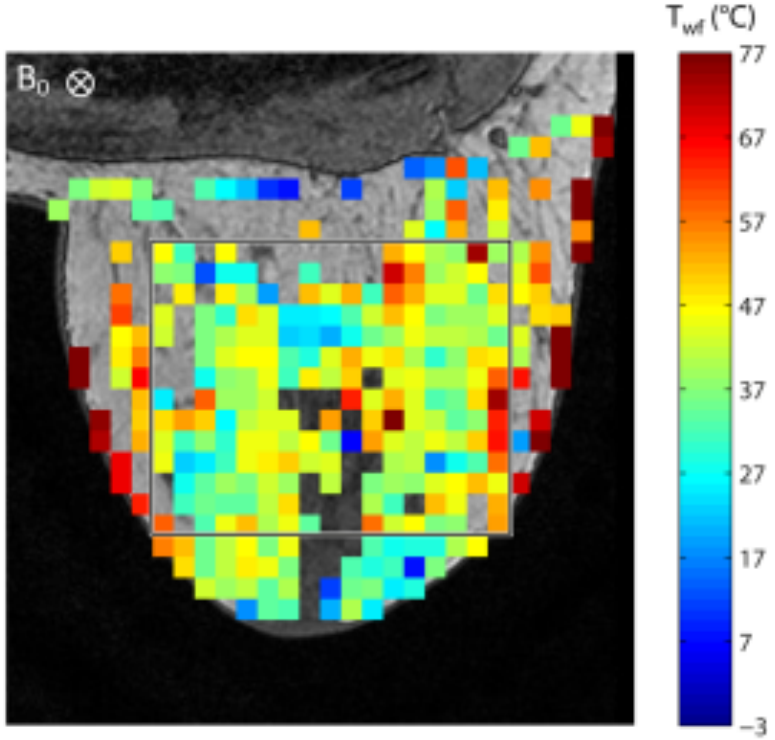




Sprinkhuizen SM, *Magn Reson Med*, 2010
Baron P, *Magn Reson Med*, 2016

# PRF Thermometry with Fat: Dixon Method

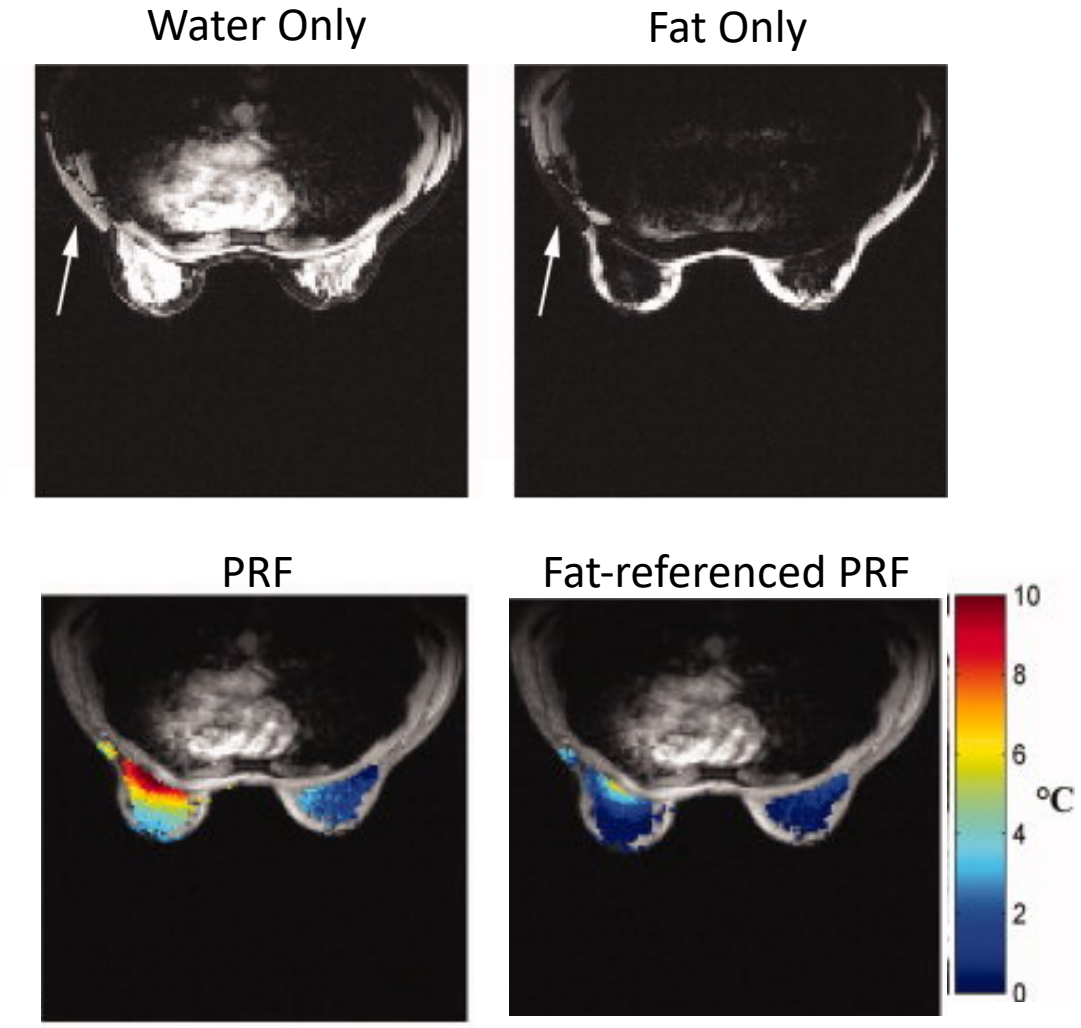


- In fat-containing pixels, the phase at a known temperature is subtracted from the phase at the elevated temperature. The net phase change is assumed to be purely caused by PRF

- The "fat" phase in a fat-free pixel at position (x,y) is interpolated from the phases in neighboring fat-containing pixels using a polynomial

$$\phi'(x,y) = a_0 + a_1 x + a_2 y + a_3 x^2 + a_4 y^2 + a_5 xy + \cdots$$

and this phantom reference is used to correct for the PRF phase change in that pixel



Hofstetter LW, *J Magn Reson Imaging*, 2012

# PRF Thermometry with Fat: Referenceless

- Assuming a small heated region and a smooth-changing baseline phase map

$$\phi_b(x,y) = \Sigma_{n=0}^{N}\Sigma_{m=0}^{n-1} a(m,n) f_{m-n}(x) f_n(y)$$

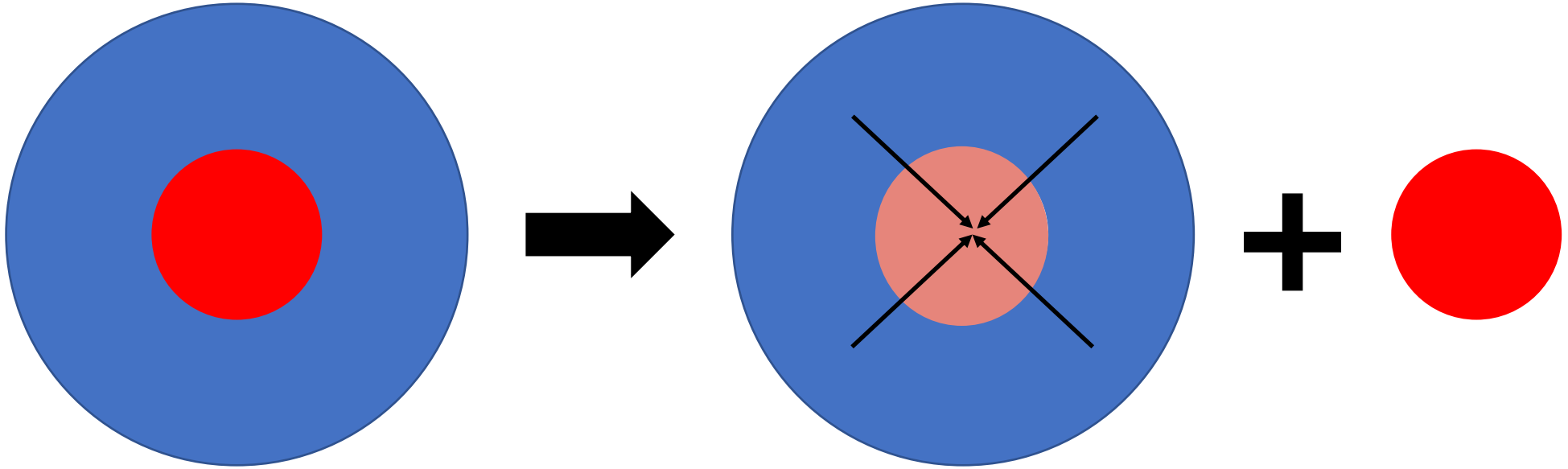

Heated phase image

Region of reference (ROR)

Region of Interest (ROI)



Rieke V, *Magn Reson Med*, 2004

# Referenceless PRF Thermometry: Phase Gradient without Phase Unwrapping

- The gradient of the phase map along both *x* and *y* directions is expanded into a polynomial

$$\nabla_x \phi_e(x,y) = \Sigma_{n=0}^{N} \Sigma_{m=0}^{n-1} a_x(m,n) f'_{m-n}(x) f_n(y)$$

- The coefficients $a_x(m,n)$ are then solved for by minimizing the $\ell_2$ norm of

$$\min_{a_x(m,n)} \Sigma_x \Sigma_y w(x,y) \left(\Delta_x \phi(x,y) - \Delta_x \phi_e(x,y)\right)^2$$

- The baseline phase map is then obtained by integrating the coefficients



Langley J, *Phys Med Biol*, 2011

# Referenceless PRF Thermometry: Reweighted $\ell_1$ without ROI

- $\ell_1$ regression is used to minimize the influence of outliers (much smaller hot spot): $\hat{\boldsymbol{a}} = \underset{\boldsymbol{a}}{\operatorname{argmin}} \Sigma_{n=1}^{N_s} ||I(x_n, y_n)|(\theta_n - \{\boldsymbol{X}\boldsymbol{a}\}_n)|$
- After each step the image is reweighted to minimize the impact of the hot spot on the overall fit

$$l = 0, \boldsymbol{W}^0 = \operatorname{diag}(|I(x_n, y_n)|)$$

$$\hat{\boldsymbol{a}}^l = \underset{\boldsymbol{a}}{\operatorname{argmin}} \parallel \boldsymbol{W}^l(\boldsymbol{\theta} - \boldsymbol{X}\boldsymbol{a}) \parallel_1$$

$$\boldsymbol{r} = \boldsymbol{\theta} - \boldsymbol{X}\hat{\boldsymbol{a}}^l$$

$$\boldsymbol{W}^{l+1} = \operatorname{diag}\left(\frac{|I(x_n, y_n|}{|r_n| + 0.01}\right)$$

until $l=l_{max}$

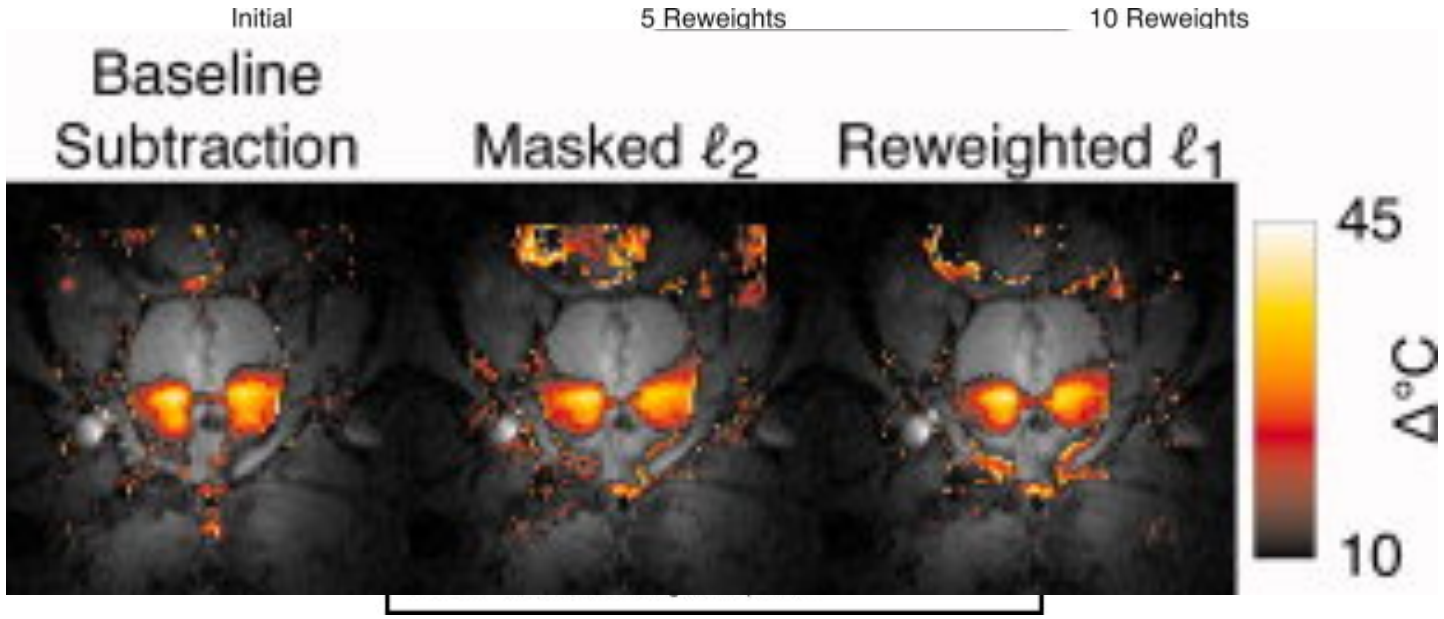




Grissom WA, *Magn Reson Med*, 2010

# More Advanced MR Thermometry Methods: Hybrid Referenceless/Multibaseline Subtraction

- The model for image voxel *j* during treatment is

$$y_j = \left( \sum_{b=1}^{N_b} x_{b,j} w_b \right) e^{i(\{Ac\}_j + \theta_j)} + \epsilon_j$$

- Iterative regularized temperature estimation is conducted to find a combination of *w*, *c* and $\vartheta$ that minimizes a cost function

$$\Psi(w, c, \theta) = \frac{1}{2} \sum_{j=1}^{N_s} \left| y_j - \left( \sum_{b=1}^{N_b} x_{b,j} w_b \right) e^{i(\{Ac\}_j + \theta_j)} \right|^2 + \lambda \parallel \theta \parallel_0$$

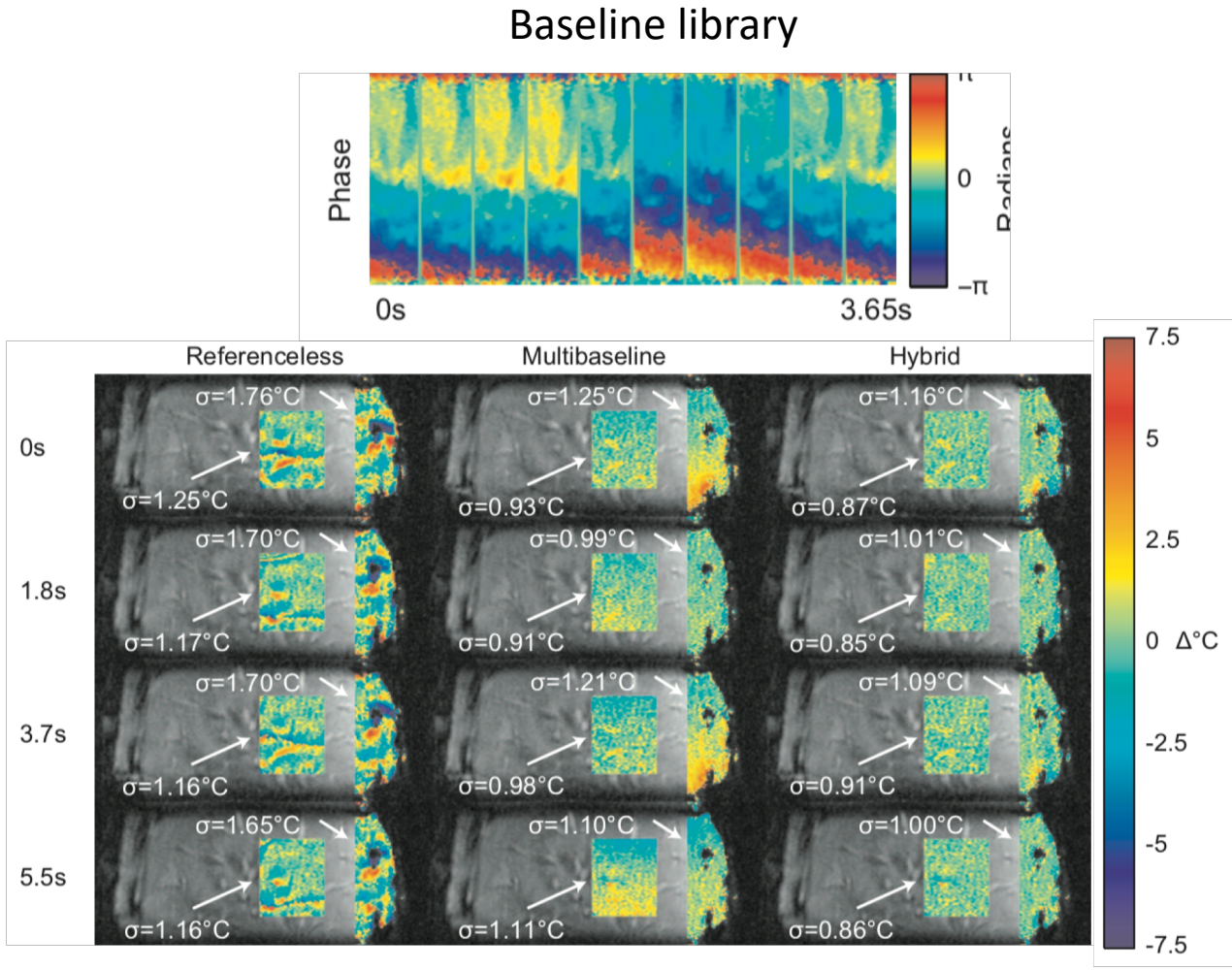




Grissom WA, *Med Phys*, 2010

# More Advanced MR Thermometry Methods: Multipathway

- Dual pathway method acquires PSIF ($p$=-1) at earlier time point during TR and FISP ($p$=0) at later time point to maximize TNR
- Temperature sensitivity of pathway p is

$$\Lambda_p = (\gamma \alpha B_0) \times (pTR + TE_p)$$

- The relative temperature changes from both pathways are combined using a weighted sum method

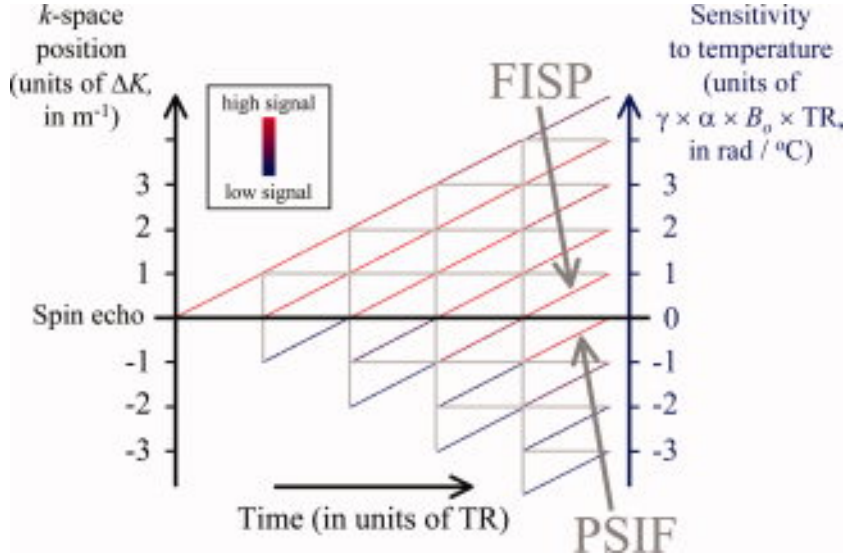


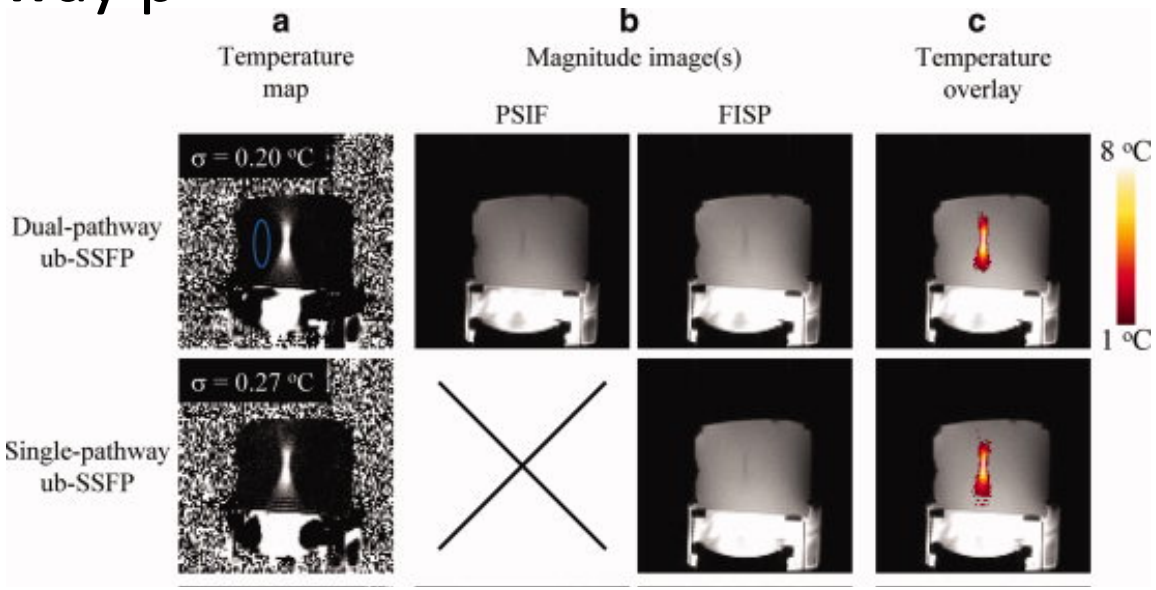




Madore B, *Magn Reson Med*, 2011

# More Advanced MR Thermometry Methods: Volumetric

Excitation and acquisition of all slices in one TR

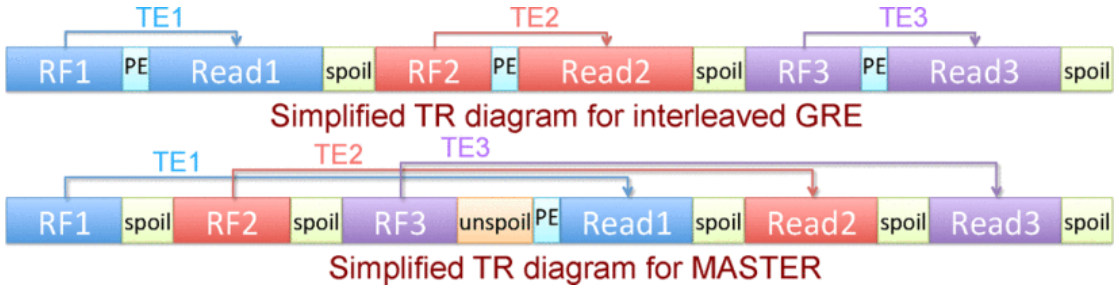


Slice Ordering

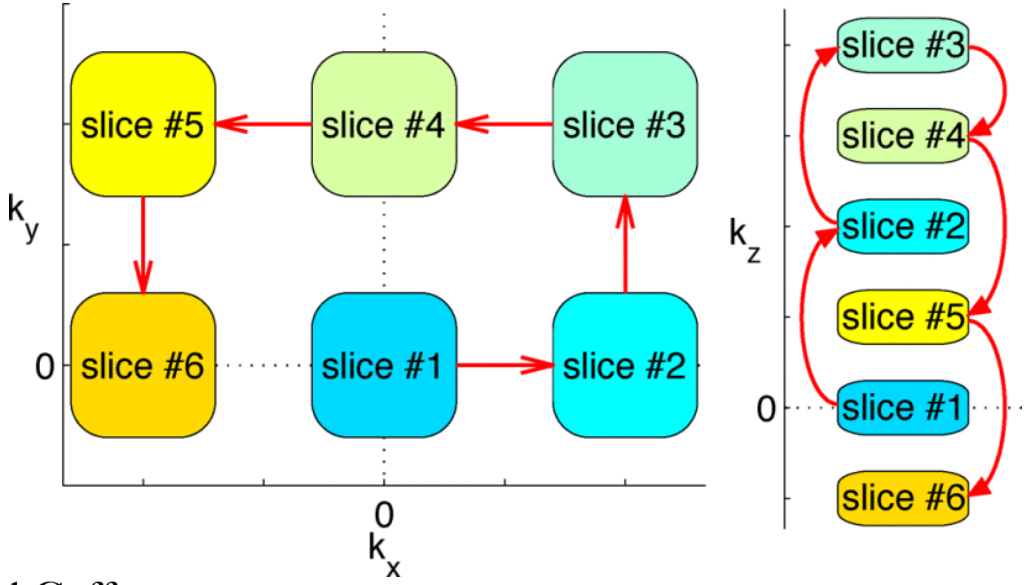


- Spoiler gradients along x and y ensure spatial separation of different slices in *k* space

Sequence performance compared with multi-slice GRE

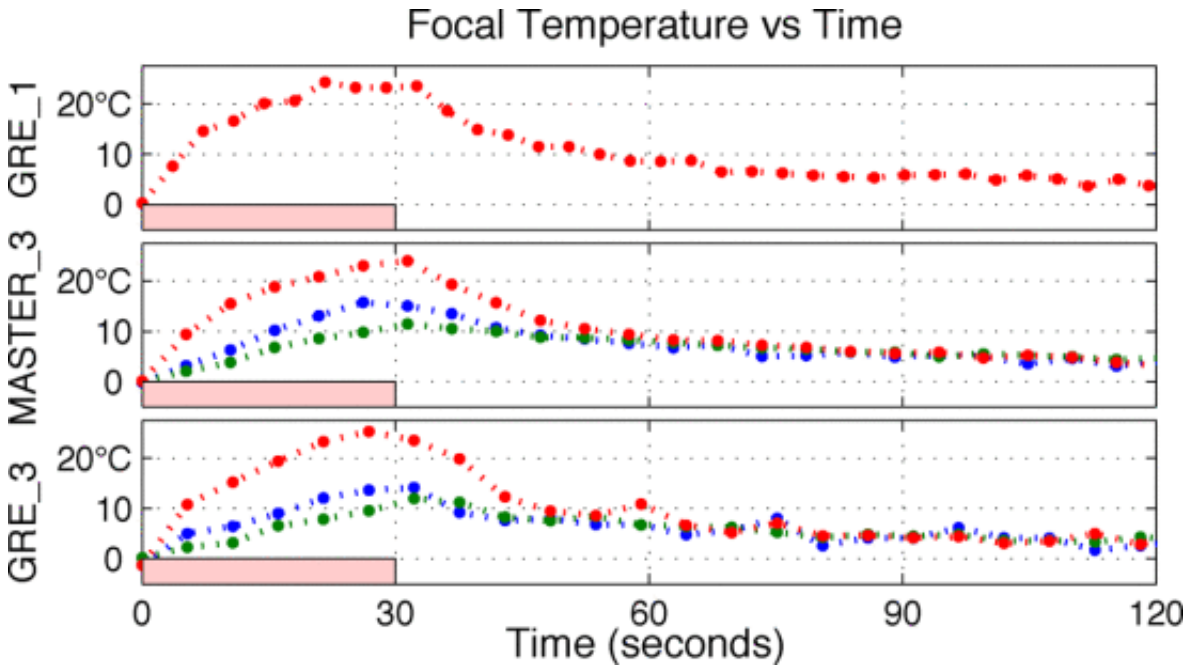


David Geffen School of Medicine

Marx M, *IEEE Trans Med Imaging*, 2015

# More Advanced MR Thermometry Methods: Undersampling & TCR

Fully sampled *k*-space: *d*

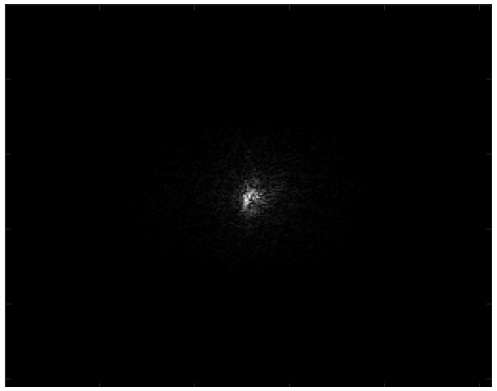

FFT

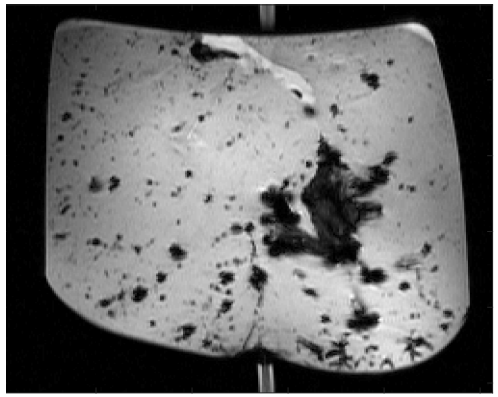

Unaliased image: *m*

Undersampled *k*-space: *d'*

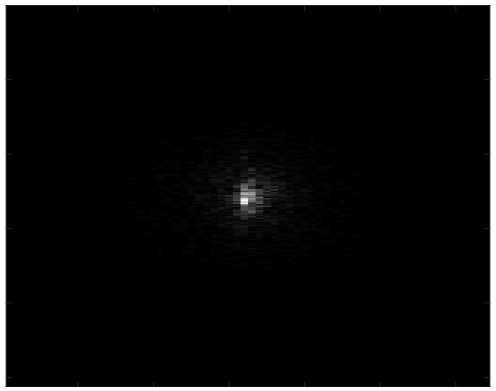

FFT

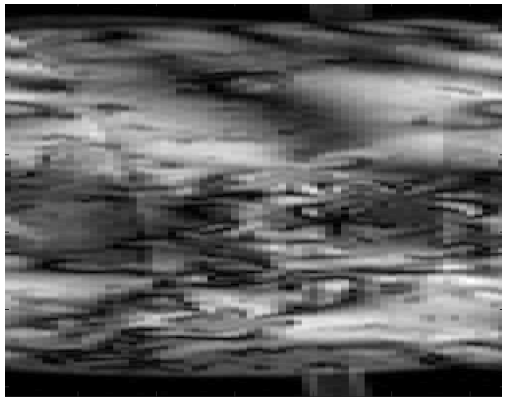

Aliased image: *m'*

- The cost function includes a fidelity term and a temporal constraint term

$$m^* = \underset{\tilde{m}}{\operatorname{argmin}}(\| WF\tilde{m} - d' \|_2^2 + \alpha\psi(\tilde{m}))$$

- For MR thermometry

$$\psi(\tilde{m}) = \sum_i^N \| \sqrt{(\nabla_t \tilde{m}_i)^2 + \beta^2} \|_1$$

Estimated image: $\tilde{m}$

Todd N, *Magn Reson Med*, 2009

# More Advanced MR Thermometry Methods: Undersampling & TCR

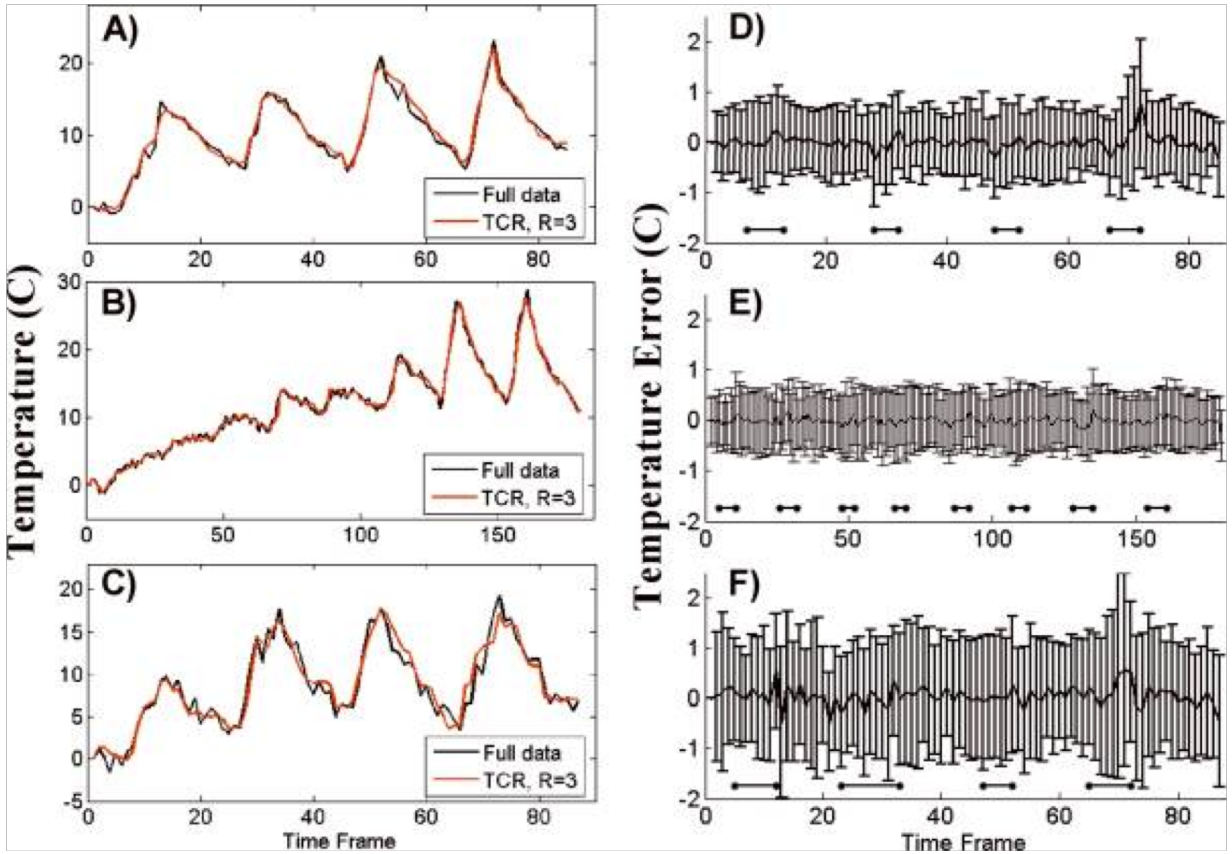


- The cost function includes a fidelity term and a temporal constraint term

$$m^* = \underset{\tilde{m}}{\operatorname{argmin}}(\| WF\tilde{m} - d' \|_2^2 + \alpha\psi(\tilde{m}))$$

- For MR thermometry

$$\psi(\tilde{m}) = \sum_i^N \| \sqrt{(\nabla_t \tilde{m}_i)^2 + \beta^2} \|_1$$

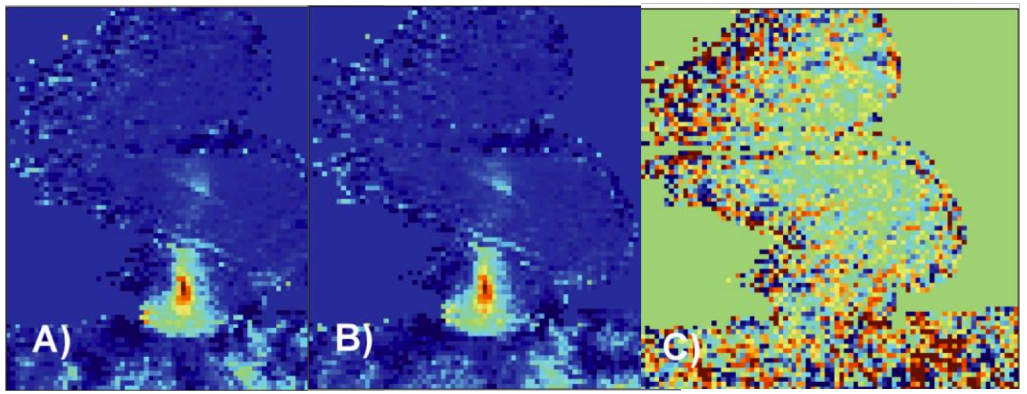


Todd N, *Magn Reson Med*, 2009

# More Advanced MR Thermometry Methods: Golden Angle Volumetric

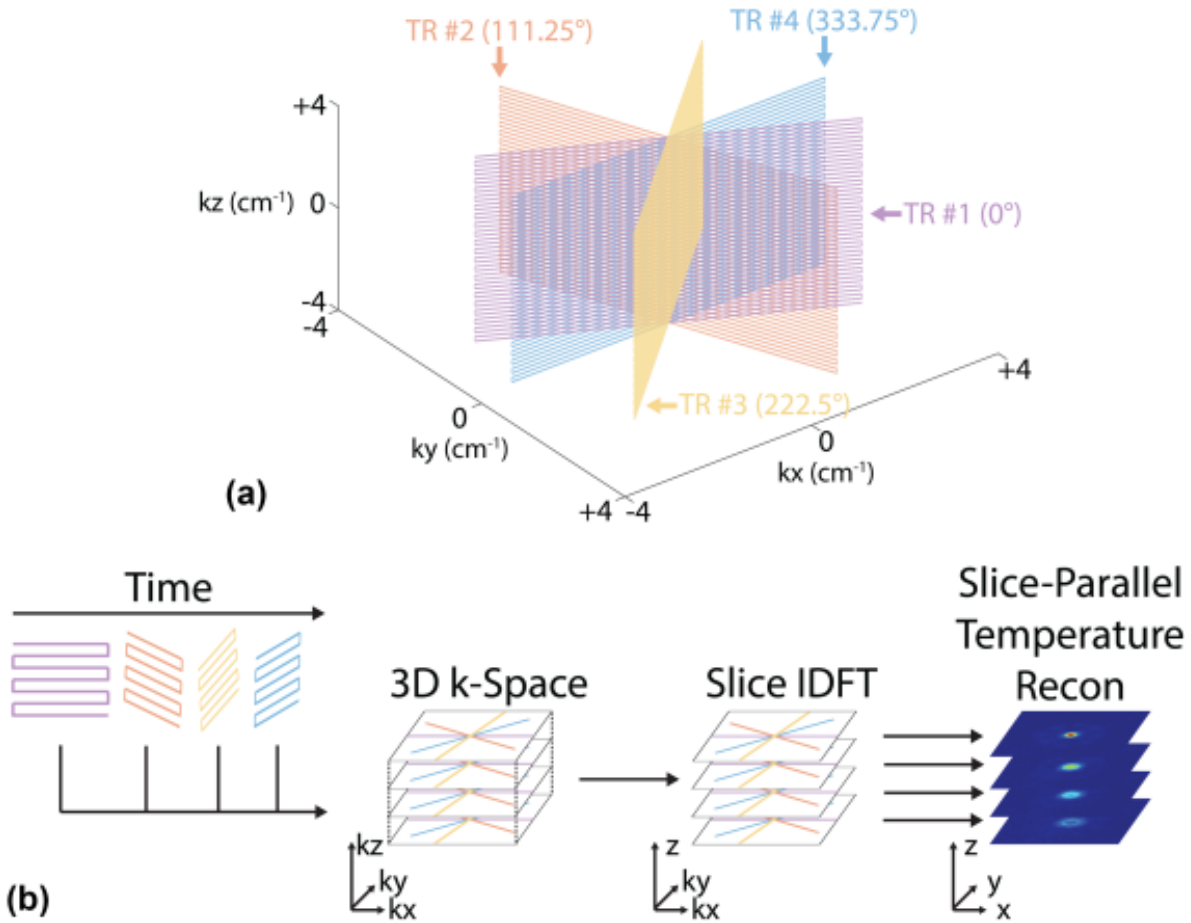


- In-plane golden angle radial encoding and through-plane Cartesian EPI encoding
- Temperature map is generated using both hybrid multibaseline/referenceless and k-space direct estimation methods

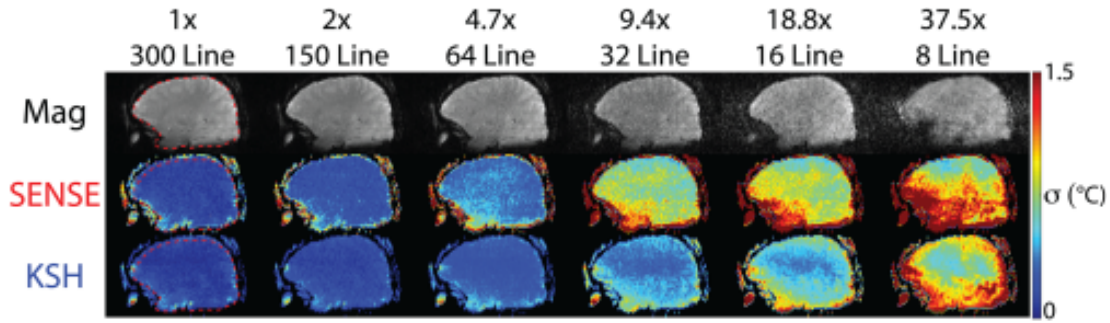




Jonathan SV, *Magn Reson Med*, 2017

# PRF Thermometry with Fat: Hybrid PRF/$T_1$

- Three-point Dixon images separate water and fat compartments
- GRE multiple echoes are combined to generate phase maps at each time step to produce temperature maps with PRF in water compartments
- $T_1$ is measured using variable flip angle (VFA) method to produce temperature maps in fatty compartments

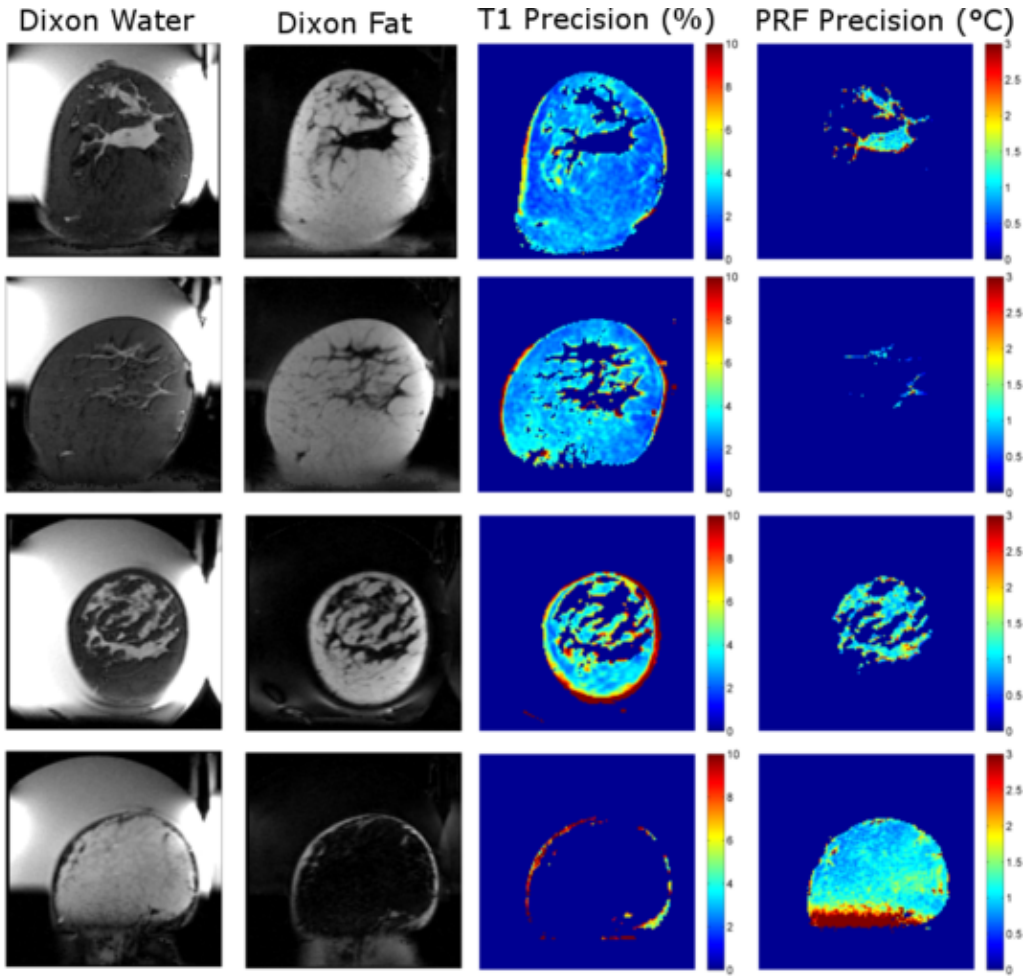




Todd N, *Magn Reson Med*, 2014

# More Advanced MR Thermometry Methods: Stack of Stars

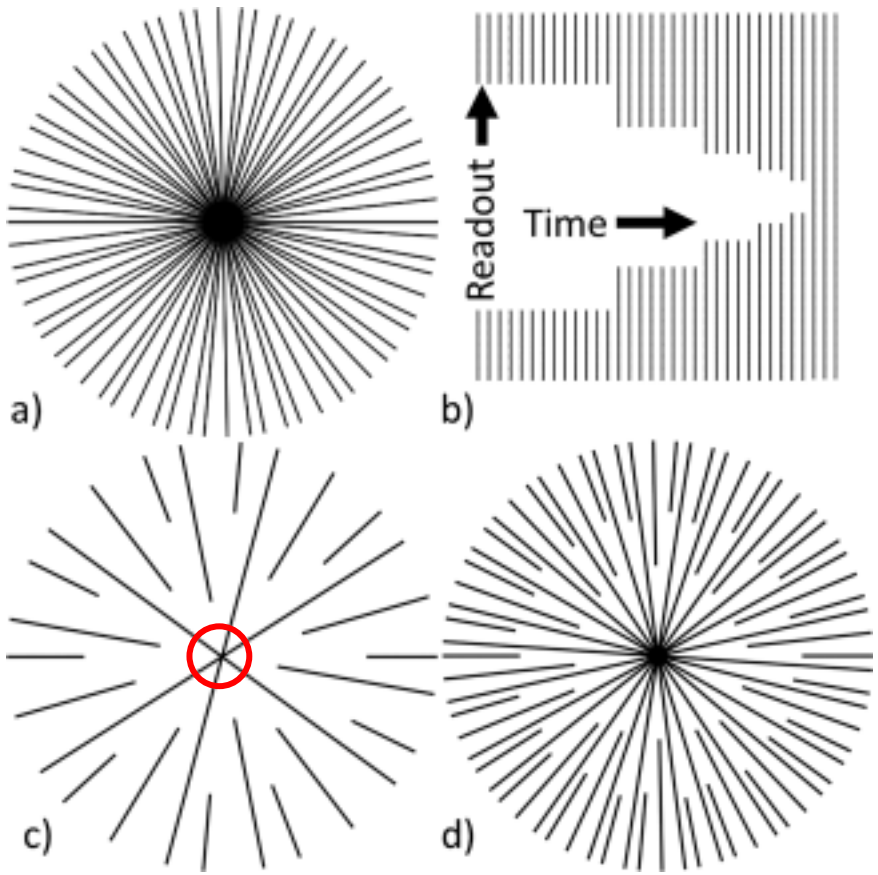


- Dipolar gradient echo acquisition scheme allows every k-space encoding step to traverse from one edge of k-space through the center to the other edge. The spoke is then rotated by the golden angle (137.56°) until sufficient coverage of k-space is met.
- Since the center of *k*-space line is acquired every TR, it has a natural robustness to motion. The k-space center can also be used as a navigator for motion correction.



Svedin BT, *Magn Reson Med*, 2017

# Radial Simultaneous PRF/$T_1$ Thermometry

- Dr. Dennis Parker's group from the University of Utah recently developed a simultaneous PRF/$T_1$ thermometry method using a radial sequence with a quasi-VFA scheme.
- The sequence acquires a reference $T_1$-weighted image at baseline temperature using one of the flip angles (e.g., smaller one $\alpha$), and then acquires a series of $T_1$-weighted images during HIFU using the other flip angle (e.g., larger one $\beta$), and the baseline $T_1$.
- Change in $T_1$ during HIFU is then calculated by deriving from the magnitude of dynamic and reference images using

$$T_1 + \Delta T_1 = \frac{1 - E_1}{1 - E_1\cos(\alpha)} \frac{1 - E_{1est}\cos(\alpha)}{1 - E_{1est}\cos(\beta)}$$ , with $E_1 = e^{-TR/T_1}, T_{1est} = \frac{-TR}{\ln(m)}, m = \frac{y_2 - y_1}{x_2 - x_1}$

$$y_2 = \frac{S_2}{\sin(\beta)}, y_1 = \frac{S_1}{\sin(\alpha)}, x_2 = \frac{S_2}{\tan(\beta)}, x_1 = \frac{S_1}{\tan(\alpha)}$$

Svedin BT, *Magn Reson Med*, 2019

# Radial Simultaneous PRF/$T_1$ Thermometry

- With the application of KWIC filter, the method could produce a 3D set of PRF/$T_1$ map every 2s in cadaver and human volunteers.
- But the calculation of $T_1$ leaves the method susceptible to bulk motion.
- It also does not take into account the change of spin density caused by temperature.

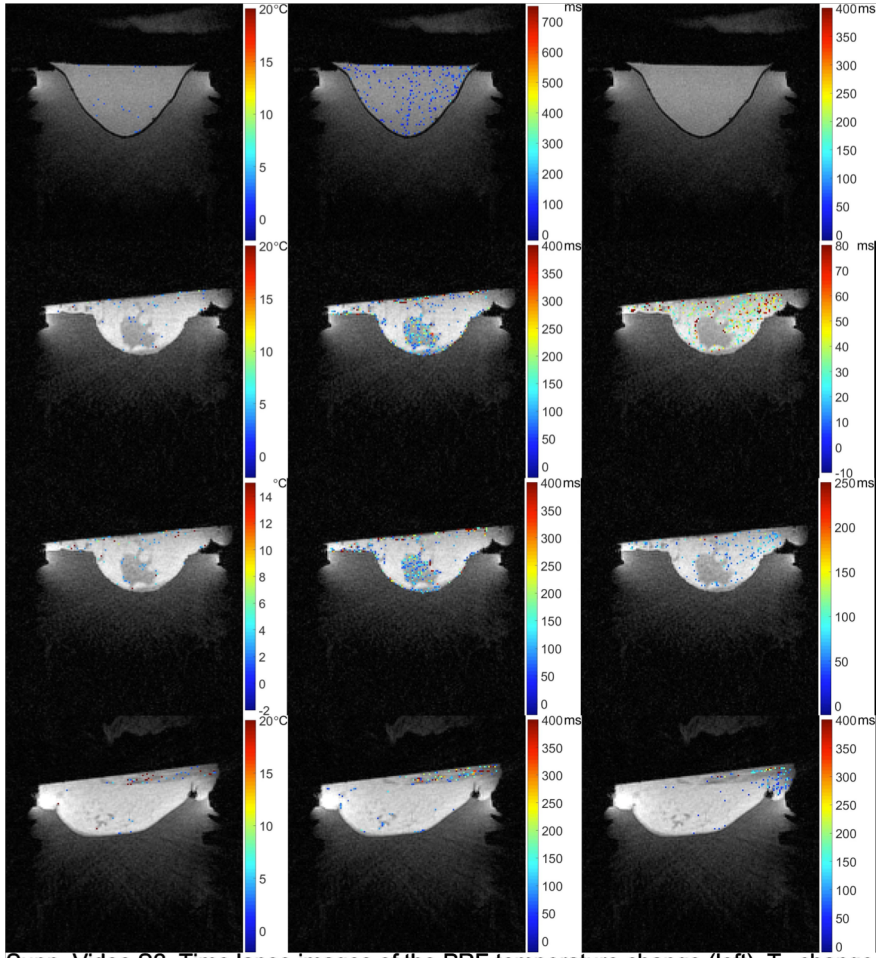

Supp. Video S2. Time lapse images of the PRF temperature change (left), $T_1$ change in aqueous tissue only (middle) and $T_1$ change in adipose tissue only (right) for the gelatin phantom (top), first (2nd row) and second (3rd row) ultrasound sonications in the first cadaver breast and for the second cadaver breast (bottom row)



Svedin BT, *Magn Reson Med*, 2019

# Summary

- MR thermometry has been successfully implemented in multiple clinical studies, including breast, prostate, liver and rectal cancer.
- Various methodologies for better and faster temperature measurement using MRI are presented here. PRF still remains the most robust method, but combining PRF with $T_1$ has also yielded promising results in mixed muscle and fatty tissues under HIFU ablation.
- The sensitivity of the PRF method to motion, perfusion and susceptibility changes, as well as the inability to measure temperatures in fatty tissue, are remaining challenges to improving accuracy and expanding its clinical potential.